SIAM J. IMAGING SCIENCES
Vol. 7, No. 1, pp. 337–365

Geometric Registration of High-Genus Surfaces*

Lok Ming Lui† and Chengfeng Wen†

Abstract. This paper presents a method of obtaining geometric registrations between high-genus ($g \geq 1$) surfaces. Surface registration between simple surfaces, such as simply connected open surfaces, has been well studied. However, very few works have been carried out for the registration of high-genus surfaces. The high-genus topology of the surface poses a great challenge for surface registration. A possible approach is to partition surfaces into simply connected patches and registration can be done in a patch-by-patch manner. Consistent cuts are required, which are usually difficult to obtain and prone to error. In this work, we propose an effective way to obtain geometric registration between high-genus surfaces without introducing consistent cuts. The key idea is to conformally parameterize the surface into its universal covering space, which is either the Euclidean plane or the hyperbolic disk embedded in $\mathbb{R}^2$. Registration can then be done on the universal covering space by iteratively minimizing a shape mismatching energy measuring the geometric dissimilarity between the two surfaces. The Beltrami coefficient of the mapping is considered and adjusted in order to control the bijectivity of the mappings in each iteration. Our proposed algorithm effectively computes a smooth registration between high-genus surfaces that matches geometric information as much as possible. The algorithm can also be applied to find a smooth registration minimizing any general energy functionals. Numerical experiments on high-genus surface data show that our proposed method is effective for registering high-genus surfaces with geometric matching. We also applied the method to register anatomical structures for medical imaging, which demonstrates the usefulness of the proposed algorithm.

Key words. surface registration, high-genus surface, universal covering space, conformal parameterization, shape mismatching energy

AMS subject classifications. 65D18, 68U05

DOI. 10.1137/130932053

1. Introduction.

Registration refers to the process of finding an optimal 1-1 correspondence between images or surfaces. It has been extensively applied to different areas, such as medical imaging, computer graphics, and computer vision. For example, in medical imaging, registration is always needed for statistical shape analysis, morphometry, and processing of signals on brain surfaces (e.g., denoising or filtering), while in computer graphics, surface registration is needed for texture mapping, which aligns each vertex to a position of the texture image, to improve the visualization of the surface mesh. Developing an effective algorithm for registration is therefore very important.

Surface registration between simple surfaces, such as simply connected open surfaces or genus-0 closed surfaces, has been extensively studied. A lot of effective algorithms have been

*Received by the editors August 6, 2013; accepted for publication (in revised form) November 13, 2013; published electronically February 18, 2014.
http://www.siam.org/journals/siims/7-1/93205.html

†Department of Mathematics, The Chinese University of Hong Kong, Hong Kong (lmlui@math.cuhk.edu.hk, cfwen@math.cuhk.edu.hk). The first author's research was supported by RGC GRF (Project ID: 401811) and CUHK FIS Grant (Project ID. 1902036).

proposed. However, as far as we know, very little literature has reported on the registration between high-genus surfaces. The high-genus topology of the surfaces poses a great challenge for registering the surfaces. A possible approach for coping with high-genus surface registration is by introducing cuts to partition the surface into several simply connected patches. Registration can then be carried out in a patch-by-patch manner. As a result, consistent cuts are required, which are usually difficult to locate and prone to error. Motivated by this, we are interested in developing a geometric registration algorithm for high-genus surfaces that does not involve the introduction of boundary cuts.

In this paper, we propose an effective way to obtain registrations between high-genus surfaces without introducing any cuts that match the geometry as much as possible. The key idea is to conformally parameterize the surface into its universal covering, which is either the two dimensional (2D) Euclidean plane $\mathbb{C}$ or the hyperbolic disk $\mathbb{H}^2$, using the discrete Ricci flow method [35, 36]. Registration can then be done on the universal covering space by minimizing a shape mismatching energy measuring the geometric dissimilarity between the surfaces. Our proposed algorithm effectively computes a smooth registration between high-genus surfaces that matches the geometric information as much as possible. The algorithm can also be applied to find a smooth registration minimizing any general energy functionals. To test the performance of the proposed method, numerical experiments have been done on synthetic high-genus surface data. Results show that our proposed algorithm is effective in registering high-genus surfaces with complete geometric matching. The proposed method has also been applied to register anatomical structures for medical imaging, which demonstrates the usefulness of the proposed algorithm.

The rest of the paper is organized as follows. In section 2, we describe some previous works closely related to our paper. In section 3, we introduce some basic mathematical concepts. The proposed algorithm for high-genus surface registration is explained in detail in section 4. The detailed numerical implementation of the algorithm will be described in section 5. In section 6, we show the numerical experimental results. The conclusion and future works are described in section 7.

2. Previous works.

In this section, we will describe some previous works closely related to our works.

Our proposed algorithm requires surface parameterization of the high-genus surface onto its universal covering space. Surface parameterization has been extensively studied, and different algorithms have been proposed. Conformal registration, which minimizes angular distortion, has been widely used to obtain a smooth 1-1 correspondence between surfaces [4, 5, 7, 1, 16, 6]. For example, Hurdal and Stephenson [16] proposed computing the conformal parameterizations using circle packing and applied it to registration of human brains. Gu et al. (see [5, 7, 6]) proposed computing the conformal parameterizations of human brain surfaces for registration using harmonic energy minimization and holomorphic 1-forms. Conformal registration is advantageous since it preserves the local geometry well.

Surface registration, which aims to find an optimal 1-1 correspondence between surfaces, has also been extensively studied. Various algorithms have been proposed by different research groups. Landmark-free registration has been proposed to obtain 1-1 correspondences

between shapes without feature landmarks. Different algorithms have been proposed to obtain registrations based on the shape information (such as curvatures) defined on the surfaces. Lyttelton et al. [2] computed surface registrations with surface curvature matching. Fischl et al. [4] proposed an algorithm for brain registration that better aligns cortical folding patterns by minimizing the mean squared difference between the convexity of the surface and the average convexity across a set of subjects. Lord et al. [17] proposed matching surfaces by minimizing the deviation of the registration from isometry. Bronstein et al. [9] propose finding the registration between nonrigid shapes by solving an isometric similarity problem. Lipman et al. (see [10, 11]) proposed another similarity criterion, which is determined by solving a mass-transportation problem between surfaces' conformal density. Yeo et al. [18] proposed the spherical demons method, which adopted the diffeomorphic demons algorithm [20], for driving surfaces into correspondence based on the mean curvature and average convexity. Quasi-conformal mappings have been applied to obtain surface registration with bounded conformality distortion [27, 29, 28, 30]. For example, Lui et al. [29] proposed computing quasi-conformal registrations between hippocampal surfaces based on the holomorphic Beltrami flow method, which matches geometric quantities (such as curvatures) and minimizes the conformality distortion [27]. Most of the above registration algorithms cannot match feature landmarks, such as sulcal landmarks on the human brains, consistently. To alleviate this issue, landmark-matching registration algorithms are proposed by various research groups. Bookstein [19] proposed obtaining a registration that matches landmarks as much as possible using a thin-plate spline regularization (or biharmonic regularization). Tosun, Rettmann, and Prince [33] proposed combining iterative closest point registration, parametric relaxation, and inverse stereographic projection to align cortical sulci across brain surfaces. These diffeomorphisms obtained can better match landmark features, although not perfectly. Wang et al. (see [21, 24]) proposed computing the optimized conformal parameterizations of brain surfaces by minimizing a compounded energy. Besides, smooth vector fields have also been proposed to represent surface maps. Lui et al. [23] proposed the use of vector fields to represent surface maps and reconstruct them through integral flow equations. They obtained shape-based landmark-matching harmonic maps by looking for the best vector fields minimizing a shape energy. The use of vector fields to represent surface maps makes optimization easier, but they cannot describe all surface maps. Time dependent vector fields can be used to represent the set of all surface maps. For example, Joshi and Miller [8] proposed the generation of large deformation diffeomorphisms for landmark point matching, where the registrations are generated as solutions to the transport equation of time dependent vector fields. The time dependent vector fields facilitate the optimization procedure, although it may not be a good representation of surface maps since it requires more memory. Later, Lin et al. [37] proposed a unified variational approach for registration of gene expression data to a neuroanatomical mouse atlas in two dimensions that matches feature landmarks. Again, landmarks cannot be exactly matched. Note that inexact landmark-matching registrations are sometimes beneficial. In the case when landmark points/curves are not entirely accurate, this method is more tolerant of errors in labeling landmarks and gives better parameterization. Most of the above algorithms deal with the registration problem between simply connected open or closed surfaces. Few works have dealt with registering high-genus surfaces.

3. Mathematical background. In this section, we describe some basic mathematical concepts related to our algorithms. For details, we refer the readers to [3, 31, 32].

A surface S with a Riemannian metric is called a *Riemann surface*. Given two Riemann surfaces M and N, a map $f : M \to N$ is *conformal* if it preserves the surface metric up to a multiplicative factor called the *conformal factor*. An immediate consequence is that every conformal map preserves angles. With the angle-preserving property, a conformal map effectively preserves the local geometry of the surface structure. Under the local coordinates of M and N, f can be expressed as $f(z) = u(z) + iv(z)$, where $z = x + iy$. Then, f is a conformal map if and only if it satisfies the Cauchy–Riemann equation

$$\frac{\partial u}{\partial x} = \frac{\partial v}{\partial y}, \quad \frac{\partial u}{\partial y} = -\frac{\partial v}{\partial x} \tag{1}$$

or, equivalently,

$$\frac{\partial f}{\partial \bar{z}} = 0. \tag{2}$$

According to the Riemann uniformization theorem, every Riemann surface admits a conformal Riemannian metric of constant Gaussian curvature. Such a metric is called the *uniformization metric*. The uniformization metric for a genus $g = 1$ surface induces 0 Gaussian curvature, whereas a genus $g > 1$ surface induces -1 Gaussian curvature, which is called the *hyperbolic metric* of the surface.

Every high-genus surface S (with genus $g \geq 1$) is associated with a universal covering space $\widehat{S} \subseteq \mathbb{R}^2$. A universal covering space is a simply connected space with a continuous surjective conformal map $\pi : \widehat{S} \to S$ satisfying the following: for any $p \in S$, there exists an open neighborhood U of p such that $\pi^{-1}(U)$ is a disjoint union of open sets in $\widehat{S}$. When $g = 1$, $\widehat{S}$ is equal to the whole plane $\mathbb{R}^2$. π is called the *covering map*. The covering map is invariant under the *deck transformation*. A deck transformation is a map $\sigma : \widehat{S} \to \widehat{S}$ such that $\pi \circ \sigma = \pi$. The collection of all deck transformations forms a group, called the *deck transformation group*, which is $2g$ dimensional. When $g > 1$, $\widehat{S}$ is the unit disk equipped with the hyperbolic metric, which is called the *Poincaré disk* $\mathbb{H}^2$. The Poincaré disk $\mathbb{H}^2$ is a unit disk equipped with a metric defined as follows:

$$ds^2 = \frac{4dzd\bar{z}}{(1 - z\bar{z})^2}. \tag{3}$$

The above metric is related to the hyperboloid model $\{(x, y, z) \mid x^2 + y^2 + 1 = z^2\}$ projectively. Suppose (x, y, z) is a point on the upper sheet of the hyperboloid. The point can be projected onto the plane $\{(x, y, z) \mid z = 0\}$ by intersecting it with a line drawn through $(0, 0, -1)$. The hyperbolic metric (3) can then be induced by this projective map.

The distance between two points z and z_0 on the Poincaré disk is given by

$$d(z, z_0) = \tanh^{-1} \left| \frac{z - z_0}{1 - z\bar{z_0}} \right|. \tag{4}$$

All rigid motions on the Poincaré disk are *Möbius transformations*:

$$z \to e^{i\theta} \frac{z - z_0}{1 - z\bar{z_0}}, \quad z_0 \in \mathbb{D}, \quad \theta \in [0, 2\pi]. \tag{5}$$

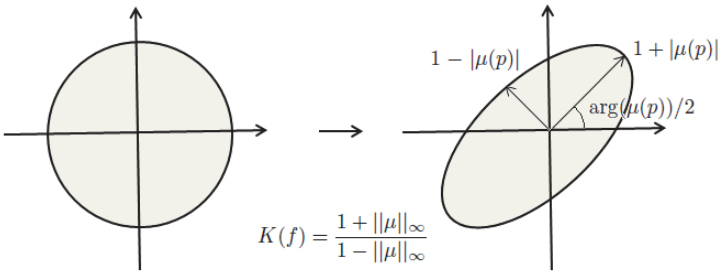

Figure 1. *Illustration of how the Beltrami coefficient determines the conformality distortion.*

Every high-genus surface can be conformally embedded into its associated universal covering space in $\mathbb{R}^2$.

Next, a natural generalization of conformal maps are *quasi-conformal* maps, which are orientation preserving homeomorphisms between Riemann surfaces with bounded conformality distortion, in the sense that their first order approximations take small circles to small ellipses of bounded eccentricity [3]. Thus, a conformal homeomorphism that maps a small circle to a small circle can also be regarded as quasi-conformal. In general, surface registrations and parameterizations can be considered as quasi-conformal maps. Mathematically, $f : \mathbb{C} \to \mathbb{C}$ is quasi-conformal provided that it satisfies the Beltrami equation

$$\frac{\partial f}{\partial \overline{z}} = \mu(z)\frac{\partial f}{\partial z} \tag{6}$$

for some complex-valued Lebesgue measurable $\mu : \mathbb{C} \to \mathbb{C}$ satisfying $||\mu||_\infty < 1$. μ is called the *Beltrami coefficient*, which is a measure of nonconformality. The Beltrami equation is a generalization of the Cauchy–Riemann equation (2). In particular, the map f is conformal around a small neighborhood of p when $\mu(p) = 0$. From $\mu(p)$, we can determine the angles of the directions of maximal magnification and shrinking and the amount of them as well. Specifically, the angle of maximal magnification is $\arg(\mu(p))/2$ with magnifying factor $1 + |\mu(p)|$; the angle of maximal shrinking is the orthogonal angle $(\arg(\mu(p)) - \pi)/2$ with shrinking factor $1 - |\mu(p)|$. The distortion or dilation is given by

$$K = (1 + |\mu(p)|)/(1 - |\mu(p)|). \tag{7}$$

Thus, the Beltrami coefficient μ gives us all the information about the properties of the map (see Figure 1).

Given a Beltrami coefficient $\mu : \mathbb{C} \to \mathbb{C}$ with $\|\mu\|_\infty < 1$, there is always a quasi-conformal mapping from $\mathbb{C}$ onto itself which satisfies the Beltrami equation in the distribution sense [3].

The Beltrami coefficient will be used in this work to control the bijectivity of the mappings in each iteration.

4. Algorithms.

In this section, we explain our algorithm for registering high-genus surfaces in detail. The basic idea is to embed the surfaces into their universal covering spaces. The computation of the surface registration can then be carried out on the universal covering

spaces in $\mathbb{R}^2$. In summary, our proposed algorithm can be divided into the following three main stages:

1. *Conformal embedding of the high-genus surface into the universal covering space:* The high-genus surfaces are first conformally parameterized into their universal covering spaces in $\mathbb{R}^2$, which is the Euclidean plane $\mathbb{R}^2$ for $g = 1$ and hyperbolic disk $\mathbb{H}^2$ for $g > 1$.
2. *Initial registration:* Harmonic registration between the fundamental domains is computed to obtain an initial surface registration.
3. *Shape matching registration:* A surface registration which matches the geometry is obtained by minimizing a shape mismatching energy on the universal covering space.

In the following, we will describe each stage in detail.

4.1. Conformal embedding of the high-genus surface into the universal covering space.

In this work, the computation of the surface registration is carried out on the universal covering spaces in $\mathbb{R}^2$ of the high-genus surfaces. This simplifies the calculation since all computations can be done in the 2D space.

The conformal embedding of S into its universal covering space $\widehat{S}$ can be computed using the Ricci flow method introduced by Gu et al. (see [35, 36]). Ricci flow is the process of conformally deforming the surface metric $g = (g_{ij}(t))$ according to its induced Gaussian curvature $K(t)$ to its uniformization metric. This process is similar to the heat flow of the metric on the manifold:

$$\frac{dg_{ij}(t)}{dt} = -2(K(t) - \bar{K})g_{ij}(t), \tag{8}$$

where $\bar{K} = 0$ $(g = 1)$ or $\bar{K} = -1$ $(g > 1)$ is target curvature. Convergence of this process is guaranteed by Hamilton's theorem. $g(\infty)$ is the desired uniformization metric.

To obtain the conformal embedding, the surface S is first sliced along the cut graph G. Let $p \in S$ be a base point on the surface S. There are many *closed loops* based at p. Two loops γ_1 and γ_2 are said to be *equivalent* if one can be deformed to the other without breaking. Mathematically, there exists a homotopy $H : [0,1] \times [0,1] \to S$ such that $H(0,\cdot) = \gamma_1$ and $H(1,\cdot) = \gamma_2$. All equivalent closed loops form an equivalence class, which can be represented by one loop. That is, we pick a closed loop in each equivalence class to represent it. The set of all equivalence classes forms a group, which is called the *fundamental group*, $\pi(S,p)$, of S. Let $\{a_1, b_1, \ldots, a_i, b_i, \ldots, a_g, b_g\}$ be a basis of $\pi(S,p)$. Suppose r, s are two elements of $\pi(S,p)$, which are two closed loops based at p. Thus, $r : [0,1] \to S$ with $r(0) = p = r(1)$ and $s : [0,1] \to S$ with $s(0) = p = s(1)$. The operation $\bullet$ of the fundamental group is the composition of two closed loops, which is defined as follows:

$$(r \bullet s)(t) = \begin{cases} r(2t), & 0 \le \mathrm{t} \le \frac{1}{2}, \\ s(2t-1), & \frac{1}{2} \le \mathrm{t} \le 1. \end{cases} \tag{9}$$

For simplicity, we write $a_i \bullet b_1$ as $a_i b_i$. The identity element is the constant map at the base point. The inverse a_i^{-1} of a loop a_i is the same loop with opposite direction at the base point. Figure 2 illustrates the basis of the fundamental group of a genus one surface and a genus two surface.

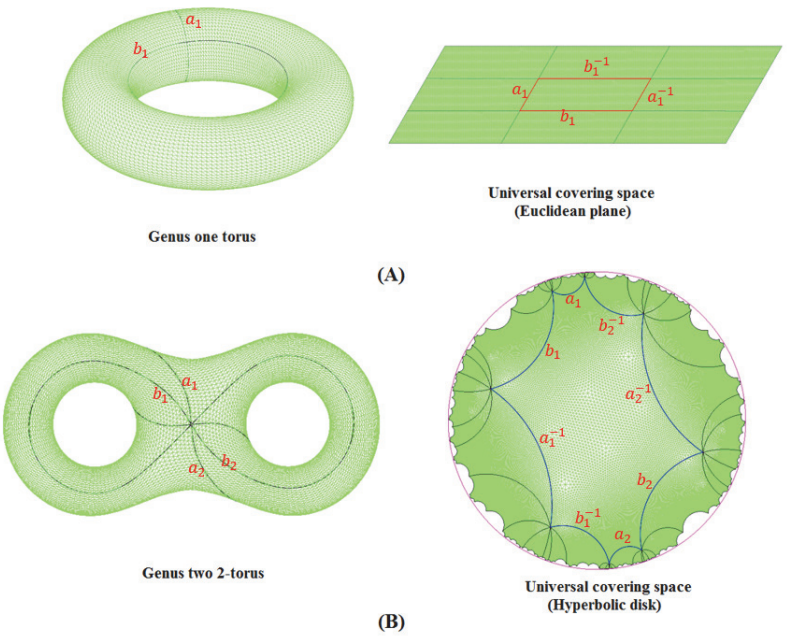

Figure 2. (A) *shows the genus one torus and its universal covering space (Euclidean plane).* (B) *shows the genus two 2-torus and its universal covering space (hyperbolic disk).*

Slicing along the basis, the high-genus surface will become a simply connected open surface, denoted by S^{cut}, which is called the *fundamental domain*.

The fundamental group basis $\{a_1, b_1, a_2, b_2, \ldots, a_g, b_g\}$ is called *canonical* if any two loops intersect only at the base point p. From algebraic topology, the boundary of the fundamental domain with respect to the canonical loops is given by

$$a_1 b_1 a_1^{-1} b_1^{-1} a_2 b_2 a_2^{-1} b_2^{-1} \cdots a_g b_g a_g^{-1} b_g^{-1}. \tag{10}$$

In this paper, we apply the greedy approach proposed in [34] to compute the homotopic basis. Each canonical cut is chosen to be the shortest path in its equivalence class.

With the uniformization metric, the fundamental domain S^{cut} can be conformally embedded onto a 2D domain $\Omega \subset \mathbb{R}^2$, called the *fundamental polygon*. By gluing copies of Ω together along its boundaries, the universal covering space of S, $\widehat{S}$, is obtained. As a result, we get the covering map $\pi : \widehat{S} \to S$ (see Figure 2). For a genus one closed surface, the universal covering space is the Euclidean plane $\mathbb{R}^2$ (see Figure 2(A)). For a genus greater than one, the universal covering space is the Poincaré disk $\mathbb{H}^2$ (see Figure 2(B)). Also, $\pi^{-1}(S) = \bigcup_{\alpha \in I} \widetilde{D}_\alpha$, where I is the index set. The fundamental polygon, Ω, belongs to one of the pieces, $\widetilde{D}_\alpha \subset \widehat{S}$. $\widetilde{D}_\alpha$ and $\widetilde{D}_\beta$ intersect at the edges if $\alpha \neq \beta$.

Note that the canonical cuts are introduced to obtain the conformal embedding of the surface into its universal covering space only. During the registration process, the canonical cuts on the source surface are allowed to move freely on the target surface since the whole process is carried out on the universal covering spaces. In other words, the correspondences

between canonical cuts are not required. It avoids the issue of finding consistent cuts to obtain an accurate registration (see Figures 5 and 11).

4.2. Initial registration between fundamental polygons. In this stage, we compute an initial surface registration between S_1 and S_2. The basic idea is to compute a harmonic map between the fundamental polygons of S_1 and S_2. An initial registration can then be obtained by the composition map.

Suppose S_1 and S_2 are conformally parameterized onto their fundamental polygons Ω_1 and Ω_2, respectively (computed in the first stage as described in section 4.1). Denote the conformal parameterizations of S_1 and S_2 by $\phi_1 : S_1 \to \Omega_1$ and $\phi_2 : S_2 \to \Omega_2$, respectively. We proceed to look for a harmonic map $\boldsymbol{h} : \Omega_1 \to \Omega_2$ between Ω_1 and Ω_2. In this subsection, the metric used is always chosen to be the Euclidean metric if genus $g = 1$ and the hyperbolic metric if $g > 1$. In the following, we always use bold letters to denote mapping.

Each fundamental polygon Ω_i of S_i $(i = 1, 2)$ has $4g$ vertices and hence $4g$ edges. Vertices of the fundamental polygon correspond to a single base point p_i on S_i. Note that the base point $p_1 \in S_1$ should correspond to the base point $p_2 \in S_2$. All edges of S_i are chosen to be geodesics.

To obtain the harmonic map $\boldsymbol{h} : \Omega_1 \to \Omega_2$, we first assign boundary correspondence $\mathfrak{h} : \partial\Omega_1 \to \partial\Omega_2$ between $\partial\Omega_1$ and $\partial\Omega_2$ ($\partial\Omega_i$ = boundary of Ω_i). Here, we assume the corresponding edges of Ω_1 and Ω_2 can be matched. The pointwise correspondence of the corresponding edges can be given by the arc-length parameterization. The boundary condition $\mathfrak{h} : \partial\Omega_1 \to \partial\Omega_2$ can then be obtained.

Note that the boundary cuts on each surface might not exactly correspond to each other. However, since canonical cuts are chosen, the edges of Ω_i correspond to the shortest loops on S_i. As a result, the initial boundary correspondence is a reasonable guess for the initial registration. We remark once again that the boundary correspondence between the boundary cuts is not constrained for our final registration. The boundary correspondence is given here just to obtain the initial registration. In the second stage, the boundary cuts on the source surface are allowed to move freely on the target surface. Hence, the correspondence between the boundary cuts is not enforced.

With the boundary correspondence $\mathfrak{h}$, a unique harmonic map between the two canonical polygons can be computed. The harmonic map $\boldsymbol{h} : \Omega_1 \to \Omega_2$ can be computed by minimizing the harmonic energy

$$E_{harmonic}(\boldsymbol{h}) = \int_{\Omega_1} |\nabla \boldsymbol{h}|^2_{\Omega_2}, \quad \text{given} \quad \boldsymbol{h}|_{\partial\Omega_1} = \mathfrak{h}. \tag{11}$$

Minimizing the above energy functional is equivalent to solving the following PDE:

$$\Delta \boldsymbol{h} = \boldsymbol{0} \ \text{ subject to } \ \boldsymbol{h}|_{\partial\Omega_1} = \mathfrak{h}, \tag{12}$$

where Δ is the Laplace–Beltrami operator under the uniformization metric.

Once $\boldsymbol{h} : \Omega_1 \to \Omega_2$ is computed, an initial registration $\boldsymbol{f}_0 : S_1 \to S_2$ can be obtained by $\boldsymbol{f}_0 := \phi_2^{-1} \circ \boldsymbol{h} \circ \phi_1$. This initial registration is a smooth mapping between S_1 and S_2. Note that there are other choices of initial maps, such as patch-by-patch registration or landmark-matching registration.

Now, to obtain a geometric matching registration, we propose iteratively adjusting the registration from the initial registration to minimize a geometric mismatching energy.

4.3. Shape matching registration. In the previous subsection, we obtained the initial registration by computing the harmonic map between the fundamental polygons. We assume that the boundary cuts are properly matched. Edges of each canonical polygon Ω_i are shortest loops on the surface S_i which pass the base point p_i. However, the shortest loops depend on the uniformization metric, which does not directly take the geometric information of the surfaces into consideration. Constraining the boundary cuts to be exactly matched often induces error in the final registration. To obtain a better geometric matching registration, we propose a variational approach, which minimizes a geometric mismatching energy, to iteratively adjust the registration without fixing the correspondences of the boundary cuts.

Surface curvatures are important quantities for describing the surface geometry. We therefore consider an energy functional which measures the curvature mismatching under a registration $\boldsymbol{f} : S_1 \to S_2$. More specifically, we propose finding an optimal diffeomorphism $\boldsymbol{f}^* : S_1 \to S_2$ which minimizes the following energy functional E_{shape}:

$$E_{shape}(\boldsymbol{f}) = \frac{1}{2}\int_{S_1} |\nabla_{g_1} \boldsymbol{f}|^2_{S_2} + \frac{\alpha^2}{2}\int_{S_1} (H_1 - H_2 \circ \boldsymbol{f})^2 + \frac{\beta^2}{2}\int_{S_1} (K_1 - K_2 \circ \boldsymbol{f})^2, \tag{13}$$

where H_1, H_2 are mean curvatures on S_1 and S_2, respectively, and K_1, K_2 are the Gaussian curvatures on S_1 and S_2, respectively.

The first term, which is the harmonic energy, controls the smoothness of the registration. The last two terms, which measure the mismatching of surface curvatures, are used to match the surface geometry.

Solving the above variational problem (13) directly on the surfaces is challenging. To simplify the optimization process, we propose solving the problem on the universal covering spaces of S_1 and S_2.

4.3.1. Optimization on universal covering spaces. Let $\boldsymbol{\pi}_1 : \widetilde{S}_1 \to S_1$ and $\boldsymbol{\pi}_2 : \widetilde{S}_2 \to S_2$ be the covering maps of S_1 and S_2, respectively. Suppose $\boldsymbol{\pi}_1^{-1}(S_1) = \bigcup_{\alpha \in I} \widetilde{D}^1_\alpha$, where I is the index set and $\widetilde{D}^1_i$ intersects with $\widetilde{D}^1_j$ at their boundaries if $i \neq j$. Similarly, we let $\boldsymbol{\pi}_2^{-1}(S_2) = \bigcup_{\beta \in I} \widetilde{D}^2_\beta$, where $\widetilde{D}^2_i$ intersects with $\widetilde{D}^2_j$ at their boundaries if $i \neq j$. We then look for a diffeomorphism $\boldsymbol{g}^* : \widetilde{S}_1 \to \widetilde{S}_2$, which is the lifting of the optimal registration $\boldsymbol{f}^* : S_1 \to S_2$ minimizing E_{shape}. In other words, we require that

$$\boldsymbol{g}^* = \boldsymbol{\pi}_2^{-1} \circ \boldsymbol{f}^* \circ \boldsymbol{\pi}_1|_{\widetilde{D}^1_\alpha} \quad \text{for any } \alpha \in U. \tag{14}$$

Equation (14) ensures that $\boldsymbol{g}^*$ satisfies the periodic condition on the covering spaces. Suppose that the canonical cuts on S_1 and S_2 are given by $\{a_1, b_1, a_2, b_2, \ldots, a_g, b_g\}$ and $\{c_1, d_1, c_2, d_2, \ldots, c_g, d_g\}$, respectively. We can find the generator $\{\varphi_1, \phi_1, \varphi_2, \phi_2, \ldots, \varphi_g, \phi_g\}$

of the deck transformation group of S_2 such that $\varphi_i(c_i) = c_i^{-1}$ and $\phi_i(d_i) = d_i^{-1}$ $(1 \le i \le g)$. $\{\varphi_1, \phi_1, \varphi_2, \phi_2, \ldots, \varphi_g, \phi_g\}$ are called the *Fuchsian group generators*. We then require that $\boldsymbol{g}^*$ satisfy the following periodic condition:

$$\varphi_i(\boldsymbol{g}^*(a_i)) = \boldsymbol{g}^*(a_i^{-1}) \quad \text{and} \quad \phi_i(\boldsymbol{g}^*(b_i)) = \boldsymbol{g}^*(b_i^{-1}). \tag{15}$$

Therefore, to obtain the optimal diffeomorphism $\boldsymbol{g}^*$, we need to minimize the following energy functional:

$$E_H(\boldsymbol{g}) = \frac{1}{2}\int_{\tilde{S}_1} |\nabla \boldsymbol{g}|^2 + \frac{\alpha^2}{2}\int_{\tilde{S}_1} (\tilde{H}_1 - \tilde{H}_2 \circ \boldsymbol{g})^2 + \frac{\beta^2}{2}\int_{\tilde{S}_1} (\tilde{K}_1 - \tilde{K}_2 \circ \boldsymbol{g})^2 \tag{16}$$

subject to the constraint that $\varphi_i(\boldsymbol{g}(a_i)) = \boldsymbol{g}(a_i^{-1})$ and $\phi_i(\boldsymbol{g}(b_i)) = \boldsymbol{g}(b_i^{-1})$ for all $1 \le i \le g$. The first term is the harmonic energy of $\boldsymbol{g}$. It is computed using the metric of universal covering space.

When $g = 1$, φ_i and ϕ_i are just translations in $\mathbb{R}^2$. When $g > 1$, φ_i and ϕ_i are Möbius transformations of the unit disk that can be computed explicitly. We will describe the computation of φ_1. The other Fuchsian group generators can be obtained in the same way. Suppose the starting and ending points of c_1 are r and s, and the starting and ending points of c_1^{-1} are s' and r'. We need to look for a Möbius transformation φ_1 such that $\varphi_1(r) = r'$ and $\varphi_1(s) = s'$. We first compute a Möbius transformation to map r to the origin, which is given by $\rho_1(z) = (z - r)/(1 - \bar{r}z)$. Then, ρ_1 maps $\overline{rs}$ to a radial Euclidean line. Let the angle between $\rho_1(\overline{rs})$ and the real axis be θ, and let $\rho_2(z) = e^{-i\theta}z$. Then, $\rho_2 \circ \rho_1$ maps r to the origin and $\overline{rs}$ to the real axis. Similarly, we can find Möbius transformations ρ_1' and ρ_2' such that $\rho_2' \circ \rho_1'$ maps r' to the origin and $\overline{r's'}$ to the real axis. The deck transformation φ_1 is then given by $\varphi_1 = \rho_1'^{-1} \circ \rho_2'^{-1} \circ \rho_2 \circ \rho_1$.

To solve the optimization problem (16), we use a splitting method to minimize

$$\begin{aligned} E_D(\boldsymbol{g}, \boldsymbol{h}) = {} & \frac{1}{2}\int_{\tilde{S}_1} |\nabla \boldsymbol{g}|^2 + \frac{\sigma^2}{2}\int_{\tilde{S}_1} |\boldsymbol{g} - \boldsymbol{h}|^2 \\ & + \frac{\alpha^2}{2}\int_{\tilde{S}_1} (\tilde{H}_1 - \tilde{H}_2 \circ \boldsymbol{h})^2 + \frac{\beta^2}{2}\int_{\tilde{S}_1} (\tilde{K}_1 - \tilde{K}_2 \circ \boldsymbol{h})^2. \end{aligned} \tag{17}$$

Fixing $\boldsymbol{g}$, we first minimize $E_1(\boldsymbol{h})$:

$$E_1(\boldsymbol{h}) = \frac{\sigma^2}{2}\int_{\tilde{S}_1} |\boldsymbol{g} - \boldsymbol{h}|^2 + \frac{\alpha^2}{2}\int_{\tilde{S}_1} (\tilde{H}_1 - \tilde{H}_2 \circ \boldsymbol{h})^2 + \frac{\beta^2}{2}\int_{\tilde{S}_1} (\tilde{K}_1 - \tilde{K}_2 \circ \boldsymbol{h})^2. \tag{18}$$

It can be done by solving the following PDE:

$$\sigma^2(\boldsymbol{g} - \boldsymbol{h}) + \alpha^2(H_1 - H_2(\boldsymbol{h}))\nabla H_2(\boldsymbol{h}) + \beta^2(K_1 - K_2(\boldsymbol{h}))\nabla K_2(\boldsymbol{h}) = 0. \tag{19}$$

In the discrete case, the above problem can be solved by the Gauss–Newton method, which will be described in section 5.

Next, fixing $\boldsymbol{h}$, we minimize

$$E_2(\boldsymbol{g}) = \frac{1}{2}\int_{\widetilde{S}_1} |\nabla \boldsymbol{g}|^2 + \frac{\sigma^2}{2}\int_{\widetilde{S}_1} |\boldsymbol{g}-\boldsymbol{h}|^2. \tag{20}$$

E_2 can be minimized by solving the elliptic PDE

$$\Delta \boldsymbol{g} - \sigma^2(\boldsymbol{g}-\boldsymbol{h}) = 0. \tag{21}$$

Recall that the registration computed should satisfy the constraint (14). Hence, we enforce this constraint when solving (21). In the discrete case, the above problem becomes a nonlinear system, which can be solved effectively using Newton's method.

In this way, we can minimize E_D alternatively over $\boldsymbol{g}$ and $\boldsymbol{h}$. More specifically, suppose $(\boldsymbol{g}_n, \boldsymbol{h}_n)$ is obtained at the nth iteration and we fix $\boldsymbol{g}_n$ to obtain $\boldsymbol{h}_{n+1}$ by solving (19). We then fix $\boldsymbol{h}_{n+1}$ to obtain $\boldsymbol{g}_{n+1}$ by solving (21).

4.3.2. Controlling bijectivity in each iteration. To control the bijectivity of the mappings in each iteration, we will consider and adjust the Beltrami coefficient of the mapping.

Let $\boldsymbol{g} : \widehat{S}_1 \to \widehat{S}_2$ be the mapping between the universal covering spaces of S_1 and S_2. We want to control the bijectivity of $\boldsymbol{g}$. Every mapping $\boldsymbol{g}$ is associated with a Beltrami coefficient, $\mu(\boldsymbol{g})$, which is a complex-valued function defined on $\widehat{S}_1$. $\boldsymbol{g}$ is bijective if and only if its Jacobian $J_{\boldsymbol{g}} > 0$ everywhere. Simple checking gives

$$J_{\boldsymbol{g}} = \left|\frac{\partial \boldsymbol{g}}{\partial z}\right|^2 (1 - |\mu(\boldsymbol{g})|^2). \tag{22}$$

Hence, $\boldsymbol{g}$ is bijective if and only if $|\mu(\boldsymbol{g})| < 1$ everywhere.

In the discrete case, we also have a similar observation. Suppose K_1 and K_2 are triangulation meshes approximating $\widehat{S}_1$ and $\widehat{S}_2$, respectively. Let $\vec{f} : K_1 \to K_2$ be a piecewise linear map (linear on each triangular face). Then, the discrete Beltrami coefficient $\vec{\mu}$, which is a complex-valued function defined on each triangular face, can be computed. According to (22), $|\vec{\mu}(T)| > 1$ on a triangular face T implies an orientation change on T. Also, the Jacobian is equal to 0 if $|\vec{\mu}(T)| = 1$, which means the map squeezes T to a point. Hence, $|\vec{\mu}(T)| < 1$ for all triangular faces T if and only if $\vec{f}$ is a piecewise linear homeomorphism without flipping.

Motivated by the above observation, we propose enforcing $\mu(\boldsymbol{g}_n) < 1$ in each iteration during the optimization process described in the last subsection. This can be done as follows. Suppose $\boldsymbol{g}_n$ is obtained at the nth iteration. Let $\epsilon > 0$ be a small parameter and $\mu_n = \mu(\boldsymbol{g}_n)$ be the Beltrami coefficient of $\boldsymbol{g}_n$. We first compute

$$\nu_n = \begin{cases} \min\{|\mu_n|, 1-\epsilon\}\frac{\mu_n}{|\mu_n|} & \text{if } |\mu_n| \neq 0, \\ 0 & \text{if } |\mu_n| = 0. \end{cases} \tag{23}$$

We then smooth ν_n by minimizing the following energy functional:

$$\int_{\widehat{S}_1} |\nabla \nu|^2 + \frac{\lambda}{2}\int_{\widehat{S}_1} |\nu - \nu_n|^2. \tag{24}$$

The above minimization problem is equivalent to solving the following PDEs:

$$\Delta\nu + \lambda(\nu - \nu_n) = 0 \tag{25}$$

subject to the constraint that for every $1 \le i \le g$, $\nu(x) = \nu(\varphi_i(x))$ for all $x \in a_i$ and $\nu(y) = \nu(\phi_i(y))$ for all $y \in b_i$.

Once a smooth Beltrami coefficient $\widetilde{\nu}_n$ is obtained, we need to find a quasi-conformal map $\boldsymbol{f}_n$ whose Beltrami coefficient closely resembles $\widetilde{\nu}_n$. Suppose $\boldsymbol{f} = \boldsymbol{u} + i\boldsymbol{v}$ with Beltrami coefficient $\mu(\boldsymbol{f}) = \rho + i\tau$. We can write $\boldsymbol{v}_x$ and $\boldsymbol{v}_y$ as linear combinations of $\boldsymbol{u}_x$ and $\boldsymbol{u}_y$,

$$\begin{aligned} -\boldsymbol{v}_y &= \alpha_1\boldsymbol{u}_x + \alpha_2\boldsymbol{u}_y, \\ \boldsymbol{v}_x &= \alpha_2\boldsymbol{u}_x + \alpha_3\boldsymbol{u}_y, \end{aligned} \tag{26}$$

where $\alpha_1 = \frac{(\rho-1)^2+\tau^2}{1-\rho^2-\tau^2}$, $\alpha_2 = -\frac{2\tau}{1-\rho^2-\tau^2}$, $\alpha_3 = \frac{(1+\rho)^2+\tau^2}{1-\rho^2-\tau^2}$.

Similarly,

$$\begin{aligned} \boldsymbol{u}_y &= \alpha_1\boldsymbol{v}_x + \alpha_2\boldsymbol{v}_y, \\ -\boldsymbol{u}_x &= \alpha_2\boldsymbol{v}_x + \alpha_3\boldsymbol{v}_y. \end{aligned} \tag{27}$$

Since $\nabla \cdot \begin{pmatrix} -\boldsymbol{v}_y \\ \boldsymbol{v}_x \end{pmatrix} = 0$, we obtain

$$\nabla \cdot \left(D \begin{pmatrix} \boldsymbol{u}_x \\ \boldsymbol{u}_y \end{pmatrix} \right) = 0 \quad \text{and} \quad \nabla \cdot \left(D \begin{pmatrix} \boldsymbol{v}_x \\ \boldsymbol{v}_y \end{pmatrix} \right) = 0, \tag{28}$$

where $D = \begin{pmatrix} \alpha_1 & \alpha_2 \\ \alpha_2 & \alpha_3 \end{pmatrix}$.

In fact, (28) is the Laplace equation under the auxiliary metric $|dz + \mu d\bar{z}|^2$ on $\widehat{S}_1$, where $|dz|^2$ and $|dw|^2$ are the Euclidean or hyperbolic metrics under the local coordinates of $\widehat{S}_1$ and $\widehat{S}_2$, respectively. Solving (28) is equivalent to finding the generalized harmonic map between $\widehat{S}_1$ and $\widehat{S}_2$ under the auxiliary metric on $\widehat{S}_1$. The generalized harmonic map between $(\widehat{S}_1, |dz + \mu d\bar{z}|^2)$ and $(\widehat{S}_2, |dw|^2)$ is unique in each homotopic class since the curvature of $\widehat{S}_2$ is 0 or -1 (≤ 0) under the uniformization metric $|dw|^2$ of the high-genus surface $\widehat{S}_2$. Also, the unique generalized harmonic map is conformal if and only if $(\widehat{S}_1, |dz + \mu d\bar{z}|^2)$ and $(\widehat{S}_2, |dw|^2)$ are conformally equivalent. In fact, $\boldsymbol{f} : (\widehat{S}_1, |dz + \mu d\bar{z}|^2) \to (\widehat{S}_2, |dw|^2)$ is conformal under the auxiliary metric on $\widehat{S}_1$. Thus, solving (28) subject to one homotopic class gives the unique conformal map $\boldsymbol{f} : (\widehat{S}_1, |dz + \mu d\bar{z}|^2) \to (\widehat{S}_2, |dw|^2)$, which is the quasi-conformal map $\boldsymbol{f} : (\widehat{S}_1, |dz|^2) \to (\widehat{S}_2, |dw|^2)$ with Beltrami differential μ under the original metric $|dz|^2$ on $\widehat{S}_1$.

Therefore, to construct $\boldsymbol{f}_n$, we let $\mu = \widetilde{\nu}_n$ and solve (28) subject to the constraint that $\varphi_i(\boldsymbol{f}_n(a_i)) = \boldsymbol{f}_n(a_i^{-1})$ and $\phi_i(\boldsymbol{f}_n(b_i)) = \boldsymbol{f}_n(b_i^{-1})$ for all $1 \le i \le g$. The details of the numerical implementation for solving (28) in the discrete case will be explained in section 5. It is our ongoing work to prove that the discrete map obtained from solving the discretization of (28) converges to the continuous quasi-conformal (hence bijective) map as the mesh size tends to 0. In practice, it is found that the obtained discrete map $\boldsymbol{f}_n$ by solving (28) has Beltrami coefficient $\vec{\mu}(\boldsymbol{f}_n)$ with supreme norm strictly less than 1 in all of our experiments. According to the above discussion, the discrete map has no flipping (bijective) in each iteration.

4.3.3. Summary of the algorithm. We now summarize our proposed high-genus surface registration algorithm as follows.

Algorithm 1 : *(High-genus surface registration)*
Input : *High-genus surfaces* S_1 *and* S_2
Output : *Geometric matching surface registration* $\boldsymbol{f} : S_1 \to S_2$

1. *Compute the conformal parameterizations* $\boldsymbol{\phi}_1 : S_1 \to \Omega_1$ *and* $\boldsymbol{\phi}_2 : S_2 \to \Omega_2$ *of* S_1 *and* S_2*, respectively.*
2. *Compute the initial mapping* f_0*; let* $\boldsymbol{g}_0 = \boldsymbol{h}_0 = \boldsymbol{f}_0$.
3. *Given* $(\boldsymbol{g}_n, \boldsymbol{h}_n)$ *at the* n*th iteration, obtain* $\boldsymbol{h}_{n+1}$ *by fixing* $\boldsymbol{g}_n$ *and solve* (19)*; fixing* $\boldsymbol{h}_{n+1}$*, obtain* $\boldsymbol{g}_{n+1}$ *by solving* (21).
4. *Compute the Beltrami coefficient* μ_{n+1} *of* $\boldsymbol{g}_{n+1}$*; obtain a smooth Beltrami coefficient* $\widetilde{\nu}_{n+1}$ *by solving* (23) *and* (25).
5. *Obtain a quasi-conformal map* $\boldsymbol{f}_{n+1}$ *from* $\widetilde{\nu}_{n+1}$ *by solving* (28).
6. *If* $||E_D(\boldsymbol{f}_{n+1}) - E_D(\boldsymbol{f}_n)|| \geq \epsilon$*, continue. Otherwise, stop the iteration.*

5. Numerical implementation.

In this section, we describe in detail the numerical implementation of our proposed algorithm. All our computations are carried out on the universal covering space, which is $\mathbb{R}^2$ when $g = 1$ and $\mathbb{H}^2$ when $g > 1$. The universal covering space consists of infinite copies of fundamental polygons, which are unique up to deck transformations. Many important operators are identical on each fundamental polygon. For example, the Laplace–Beltrami operator, which is crucial in our model, is identical on each fundamental polygon since it is invariant under rigid motions. Based on this observation, the numerical implementation can be done on one piece of the fundamental polygon, while allowing its boundary to move freely on the universal covering space of the target surface. In other words, boundary correspondences between the canonical cuts of the two surfaces are not required.

5.1. Poisson's equation on the universal covering space.

The Laplace–Beltrami operator plays a crucial role in our proposed algorithm. Most key steps involve solving Poisson's equation on the universal covering space. In this subsection, we describe how to discretize the Laplace–Beltrami operator on the fundamental polygon, which can be lifted to the universal covering space. Poisson's equation can then be solved on the universal covering space.

On a triangular mesh, the Laplace–Beltrami operator can be discretized by the cotangent formula

$$\Delta_M \boldsymbol{f}(z_i) = \sum_{j \in N_1(i)} w_{ij}(\boldsymbol{f}(z_j) - \boldsymbol{f}(z_i)), \tag{29}$$

where $N_1(i)$ is the set of vertex indices of the one-ring neighborhood of the vertex z_i and $w_{ij} = \frac{1}{2}(\cot\alpha + \cot\beta)$, where α and β are the two angles facing the edge $[v_i, v_j]$. Here, we use z_i to denote both the ith vertex and its complex coordinates. Poisson's equation can then be expressed in a matrix form:

$$\mathrm{A}\boldsymbol{f} = \boldsymbol{b}, \tag{30}$$

where A is a square matrix with $\mathrm{A}(i,j) = w_{ij}$ and $\mathrm{A}(i,i) = -\sum_{j \in N_1(i)} w_{ij}$.

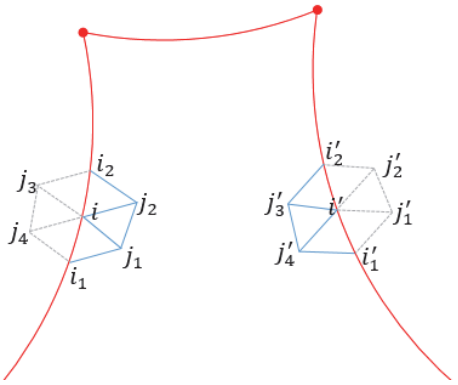

Figure 3. *Fundamental domain on the Poincaré disk.*

Note that the computation of $\Delta_M \boldsymbol{f}$ on each vertex uses only vertices in its one-ring neighborhood. For the interior vertices of the fundamental polygon Ω_1, the discretization of $\Delta_M \boldsymbol{f}$ uses vertices in Ω_1. However, for vertices on the boundary of the fundamental polygon, the discretization of $\Delta_M \boldsymbol{f}$ uses vertices outside Ω_1 (see Figure 3).

Every vertex outside the fundamental polygon has a unique copy inside the fundamental polygon up to a rigid motion. Hence, whenever vertices outside the fundamental polygon are involved, we will refer to their unique copies inside the fundamental polygon Ω_1. Note that this is also valid for vertices z_k associated with the base point $p_1 \in S_1$. That is, $z_k \in \phi_1^{-1}(p_1)$, where ϕ_1^{-1} is the inverse mapping of ϕ_1. In other words, we have a valid discretization on $z_k \in \phi_1^{-1}(p_1)$. In practice, we always fix z_k by letting $A(k,k) = 1$, $A(k,j) = 0$ if $j \neq k$, $\boldsymbol{b}(k) = \boldsymbol{f}(z_k)$ for any $z_k \in \phi_1^{-1}(p_1)$. For a vertex z_i on the boundary of Ω_1 other than points in $\phi_1^{-1}(p_1)$, the discretization can be obtained by

$$\Delta_M \boldsymbol{f}(z_i) = \sum_{j \in N_1(i)} w_{ij}(\boldsymbol{f}(z_j) - \boldsymbol{f}(z_i)) + \sum_{j \in \widetilde{N}_1(i)} w_{ij}(\boldsymbol{f}(z_j) - \boldsymbol{f}(z_i)), \tag{31}$$

where $N_1(i)$ is the set of vertex indices of one-ring neighbors of the vertex z_i on the fundamental polygon Ω_1 and $\widetilde{N}_1(i)$ is the set of vertex indices of one-ring neighbors of the vertex z_i outside the fundamental polygon. We denote further the set of vertex indices of the one-ring neighborhood of the vertex z_i inside the fundamental domain by $\overset{\circ}{N}_1(i)$. Thus, for example, in Figure 3, $N_1(i) = \{i_1, i_2, j_1, j_2\}$, $\widetilde{N}_1(i) = \{j_3, j_4\}$, $\overset{\circ}{N}_1(i) = \{j_1, j_2\}$.

For simplicity, we let $\tilde{z}_i = \boldsymbol{f}(z_i)$. The Laplace–Beltrami operator becomes

$$\Delta_M \tilde{z}_i = \sum_{j \in N_1(i)} w_{ij}(\tilde{z}_j - \tilde{z}_i) + \sum_{j \in \widetilde{N}_1(i)} w_{ij}(\tilde{z}_j - \tilde{z}_i). \tag{32}$$

Suppose $\tilde{z}_j$ is outside the fundamental domain. We denote the inside copy of vertex $\tilde{z}_j$ by $\tilde{z}_{j'}$. Let φ be the deck transformation that moves $\tilde{z}_j$ to $\tilde{z}_{j'}$, that is, $\tilde{z}_{j'} = \varphi(\tilde{z}_j)$; then we have

$$\begin{aligned}\Delta_M \tilde{z}_i &= \sum_{j\in N_1(i)} w_{ij}(\tilde{z}_j - \tilde{z}_i) + \sum_{j\in \widetilde{N}_1(i)} w_{ij}(\tilde{z}_j - \tilde{z}_i) \\ &= \sum_{j\in N_1(i)} w_{ij}(\tilde{z}_j - \tilde{z}_i) + \sum_{j'\in \overset{\circ}{N}_1(i')} w_{i'j'}(\tilde{z}_{j'} - \tilde{z}_{i'}) \\ &= \sum_{j\in N_1(i)} w_{ij}(\tilde{z}_j - \tilde{z}_i) + \sum_{j\in \widetilde{N}_1(i)} w_{ij}(\varphi(\tilde{z}_j) - \varphi(\tilde{z}_i)).\end{aligned} \tag{33}$$

The second equality uses the fact that Laplace–Beltrami operator Δ_M is invariant under rigid motions.

With this discretization, Poisson's equation can be rewritten in the matrix form

$$\mathrm{A}\tilde{z} + Q(\tilde{z}) = b, \tag{34}$$

where A is the matrix representation of the Laplace–Beltrami operator, and $Q(i,j)$ is the deck transformation that transforms outside neighbor z_j of vertex z_i to its inside copy $z_{j'}$ and is zero elsewhere, multiplied by w_{ij}.

For genus one surfaces, deck transformations are linear translations, and so Q is a linear operator. Combining Q into A, (34) becomes a linear system and can be solved efficiently.

However, for higher genus surfaces ($g > 1$), deck transformations are Möbius transformations, which are nonlinear. Equation (34) becomes a nonlinear system. It can be solved by Newton's method efficiently. Let $F(\tilde{z}) = \mathrm{A}\tilde{z} + Q(\tilde{z}) - b$. The gradient of F is given by $\nabla F = \mathrm{A} + Q'$. The problem can then be solved using the standard Newton method:

1. Initialize $\tilde{z}$ by $\tilde{z}_0$.
2. Compute $F(\tilde{z}) = \mathrm{A}\tilde{z} + Q(\tilde{z}) - b$. If $\|F(\tilde{z})\| < \epsilon$, stop the process.
3. Compute $\nabla F(\tilde{z}) = \mathrm{A} + Q'(\tilde{z})$, and solve s from equation $\nabla F(\tilde{z}) \cdot s = F(\tilde{z})$. If $\|s\| < \epsilon$, stop the process. Otherwise, let $\tilde{z} = \tilde{z} - s$ and go to step 2.

The linear equation in step 3 can be solved by LU factorization, which turns out to be quite efficient. In our numerical computation, we observe that Newton's method converges very quickly: usually two or three iterations will achieve 10^{-10} accuracy.

5.2. Solving energy minimizing problem. We use an alternating approach to minimize the proposed energy functional E_D. In each iteration, we first minimize $E_1(\boldsymbol{h})$ to get $\boldsymbol{h}$ and then minimize $E_2(\boldsymbol{g})$ to get $\boldsymbol{g}$.

We first discuss the minimization of $E_1(\boldsymbol{h})$.

At each point $p \in \widehat{S}_1$, we consider Taylor's expansion of H_2 and K_2 about $\boldsymbol{g}(p)$. For simplicity, we denote $\boldsymbol{g}(p)$ as $\boldsymbol{g}_p$ and $\boldsymbol{h}(p)$ as $\boldsymbol{h}_p$:

$$\begin{aligned}H_2(\boldsymbol{h}_p) &\approx H_2(\boldsymbol{g}_p) + \nabla H_2(\boldsymbol{g}_p) \cdot (\boldsymbol{h}_p - \boldsymbol{g}_p), \\ K_2(\boldsymbol{h}_p) &\approx K_2(\boldsymbol{g}_p) + \nabla K_2(\boldsymbol{g}_p) \cdot (\boldsymbol{h}_p - \boldsymbol{g}_p).\end{aligned} \tag{35}$$

With the linear approximation (35), we have

$$
\begin{aligned}
E_1(\boldsymbol{h}) = \frac{\sigma^2}{2}\int_{\widetilde{S}_1} |\boldsymbol{g}-\boldsymbol{h}|^2 \\
+ \frac{\alpha^2}{2}\int_{\widetilde{S}_1} (\tilde{H}_1 - \tilde{H}_2(\boldsymbol{g}) - \nabla\tilde{H}_2(\boldsymbol{g})\cdot(\boldsymbol{h}-\boldsymbol{g}))^2 \\
+ \frac{\beta^2}{2}\int_{\widetilde{S}_1} (\tilde{K}_1 - \tilde{K}_2(\boldsymbol{g}) - \nabla\tilde{K}_2(\boldsymbol{g})\cdot(\boldsymbol{h}-\boldsymbol{g}))^2 \\
= \int_{\widetilde{S}_1} \left\| \begin{pmatrix} \alpha(\tilde{H}_1 - \tilde{H}_2(\boldsymbol{g})) \\ \beta(\tilde{K}_1 - \tilde{K}_2(\boldsymbol{g})) \\ 0 \end{pmatrix} - \begin{pmatrix} \alpha\nabla\tilde{H}_2(\boldsymbol{g}) \\ \beta\nabla\tilde{K}_2(\boldsymbol{g}) \\ \sigma I_{2\times 2} \end{pmatrix} (\boldsymbol{h}-\boldsymbol{g}) \right\|^2 .
\end{aligned} \tag{36}
$$

Then the minimization problem can be solved individually for each vertex p in the least squares sense:

$$
\begin{pmatrix} \alpha\nabla\tilde{H}_2(\boldsymbol{g}) \\ \beta\nabla\tilde{K}_2(\boldsymbol{g}) \\ \sigma I_{2\times 2} \end{pmatrix} (\boldsymbol{h}_p - \boldsymbol{g}_p) = \begin{pmatrix} \alpha(\tilde{H}_1 - \tilde{H}_2(\boldsymbol{g}_p)) \\ \beta(\tilde{K}_1 - \tilde{K}_2(\boldsymbol{g}_p)) \\ 0 \end{pmatrix} . \tag{37}
$$

Let

$$
S = \begin{pmatrix} \alpha\nabla\tilde{H}_2(\boldsymbol{g}_p) \\ \beta\nabla\tilde{K}_2(\boldsymbol{g}_p) \\ \sigma I_{2\times 2} \end{pmatrix}, \quad d = \begin{pmatrix} \alpha(\tilde{H}_1 - \tilde{H}_2(\boldsymbol{g}_p)) \\ \beta(\tilde{K}_1 - \tilde{K}_2(\boldsymbol{g}_p)) \\ 0 \end{pmatrix}; \tag{38}
$$

then we have

$$
\boldsymbol{h}_p = \boldsymbol{g}_p + (S^T S)^{-1}\cdot(S^T d). \tag{39}
$$

In our computation, the inversion $(S^TS)^{-1}$ can be obtained by the Sherman–Morrison formula. Let $u^T = \frac{\alpha}{\sigma}\nabla\tilde{H}_2(\boldsymbol{g})$, $v^T = \frac{\alpha}{\sigma}\nabla\tilde{K}_2(\boldsymbol{g})$; then $S = \sigma(u, v, I_{2\times 2})^T$, $S^TS = \sigma^2(I_{2\times 2} + uu^T + vv^T)$. Applying the Sherman–Morrison formula twice, we have

$$
(S^TS)^{-1} = \frac{1}{\sigma^2}\left(I_{2\times 2} - \frac{uu^T + vv^T + (u^T\cdot v^\perp)^2 I_{2\times 2}}{1 + u^Tu + v^Tv + (u^T\cdot v^\perp)^2} \right). \tag{40}
$$

Hence we have a simple solution for $\boldsymbol{h}$. If we consider only either the mean curvature H or Gaussian curvature K (that is, $\beta = 0$ or $\alpha = 0$), the expression of $\boldsymbol{h}$ can be further simplified. For example, if $\beta = 0$, we have

$$
(S^TS)^{-1} = \frac{1}{\sigma^2}\left(I - \frac{uu^T}{1 + u^Tu} \right) \tag{41}
$$

and hence

$$
\boldsymbol{h}_p = \boldsymbol{g}_p + \frac{(\tilde{H}_1 - \tilde{H}_2(\boldsymbol{g}_p))\nabla\tilde{H}_2(\boldsymbol{g}_p)}{\frac{\sigma^2}{\alpha^2} + \nabla\tilde{H}_2(\boldsymbol{g}_p)^T\nabla\tilde{H}_2(\boldsymbol{g}_p)}. \tag{42}
$$

Next, the minimization of $E_2(\boldsymbol{g})$ can be done easily by solving (21):

$$\Delta \boldsymbol{g} - \sigma^2(\boldsymbol{g} - \boldsymbol{h}) = 0, \tag{43}$$

where Laplace–Beltrami operator Δ is discretized using the cotangent formula.

The procedure discussed in section 5.1 can be applied to solving (43). More specifically, we have to solve the following equation:

$$(\mathrm{A} - \sigma^2 \mathrm{I})\boldsymbol{g} + \mathrm{Q}(\boldsymbol{g}) = -\sigma^2 \boldsymbol{h}. \tag{44}$$

For genus one surfaces, (44) is a linear system and can be solved efficiently by a linear solver. For higher genus surfaces ($g > 1$), (44) becomes a nonlinear equation and it can be solved by Newton's method.

5.3. Solving Beltrami equation. To preserve the bijectivity of the mappings, a smoothing operation on the Beltrami coefficient is applied. A mapping is then reconstructed from the smoothed Beltrami coefficient by solving the Beltrami equation.

The Beltrami equation is in fact Poisson's equation with a generalized Laplace–Beltrami operator (see (28)). We can solve the equation as described in section 5.1. Since we have a generalized Laplace–Beltrami operator, the standard cotangent formula cannot be used. We use the discretization scheme proposed in [30], which also uses the one-ring neighborhood of a vertex to discretize the generalized Laplace–Beltrami operator. Hence, the method described in section 5.1 can still be applied.

More specifically, the gradient operator ∇_T can be discretized by a linear approximation. For a triangle $T = (i, j, k)$, $p_i = (x_i, y_i)^T$, $p_j = (x_j, y_j)^T$, $p_k = (x_k, y_k)^T$ the coordinates of the three vertices, let $e_i = p_k - p_j, e_j = p_i - p_k, e_k = p_j - p_i$; then we have

$$\nabla_T \boldsymbol{f}_i = \frac{1}{4a_T}(\boldsymbol{f}_i t_i + \boldsymbol{f}_j t_j + \boldsymbol{f}_k t_k), \tag{45}$$

where a_T is the area of the triangle, $t_i = e_i^{\perp}$, $t_j = e_j^{\perp}$, and $t_k = e_k^{\perp}$.

The discrete gradient operator at vertex i can then be obtained by

$$\nabla \boldsymbol{f}_i = \sum_{T \in N_i} \frac{1}{4a_T}(\boldsymbol{f}_i t_i + \boldsymbol{f}_j t_j + \boldsymbol{f}_k t_k), \tag{46}$$

where N_i is the collection of neighborhood faces attached to vertex i. Note that in the summation we omit the superscripts on $\boldsymbol{f}$ and t to avoid confusion.

Similarly, the discretization of divergence operator $\nabla\cdot$ for a vector $\boldsymbol{F} = (u, v)^T$ can be obtained by

$$\nabla \cdot \boldsymbol{F}_i = \sum_{T \in N_i} \frac{1}{4a_T}(\boldsymbol{F}_i \cdot t_i + \boldsymbol{F}_j \cdot t_j + \boldsymbol{F}_k \cdot t_k). \tag{47}$$

The discretization of (28) can be obtained by applying the above two formulas.

Following the discussion in section 5.1, the Beltrami equation can be formulated as

$$\mathrm{A}\tilde{z} + Q(\tilde{z}) = b. \tag{48}$$

The above equation is linear in the case of genus one surfaces and is nonlinear in the case of higher genus surfaces. By solving the above equation, we get a reconstructed quasi-conformal map associated with the smoothed Beltrami coefficient.

5.4. Summary. In this subsection, we summarize the numerical implementation details. Our proposed algorithm consists of three stages:

- Stage 1: Conformal embedding using the Ricci flow method. The implementation details of the Ricci flow method can be found in [7, 35, 36].
- Stage 2: Computation of the harmonic map as the initial registration. The implementation details can be found in [7].
- Stage 3: Geometric registration by minimizing an energy functional as described in section 5.2. Energy minimization is done by an alternative scheme:
  - First, minimize $E_1(\boldsymbol{h})$ while fixing $\boldsymbol{g}$. The explicit solution of the problem is shown in (39).
  - Second, minimize $E_2(\boldsymbol{g})$ while fixing $\boldsymbol{h}$ by solving elliptic PDE (21) as described in section 5.1.
  - Third, control the bijectivity by chopping and smoothing Beltrami coefficients, which is described in section 5.3.

6. Experimental results. To test the efficacy of the proposed algorithm, experiments have been carried out on synthetic high-genus surface data together with real medical data (vertebrae bone and vestibular system).

6.1. Synthetic surface data. We first test our algorithm on synthetic surface data.

Example 1. In our first examples, we test the proposed method on a standard torus of genus one. Figures 4(A) and (B) show two genus-1 tori, denoted by S_1 and S_2, respectively, with different intensity functions defined on each of them. The two surfaces are parameterized onto their universal covering spaces, and registration between the two surfaces is computed on the 2D parameter domains. The intensity functions on each surface are plotted on their universal covering spaces, which are shown in (C) and (D). Figure 5(A) shows the registration result that

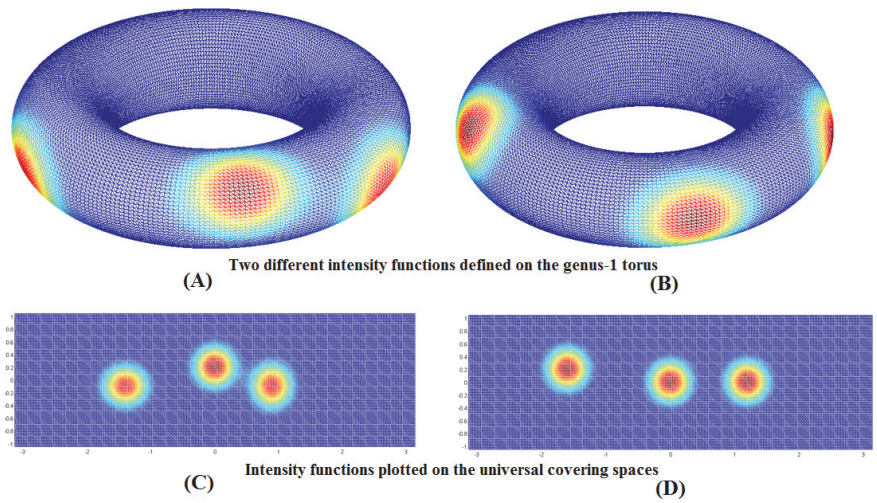

Figure 4. (A) *and* (B) *show two genus-*1 *tori with different intensity functions defined on each of them.* (C) *and* (D) *show the intensity functions plotted on the universal covering spaces of* (A) *and* (B)*, respectively.*

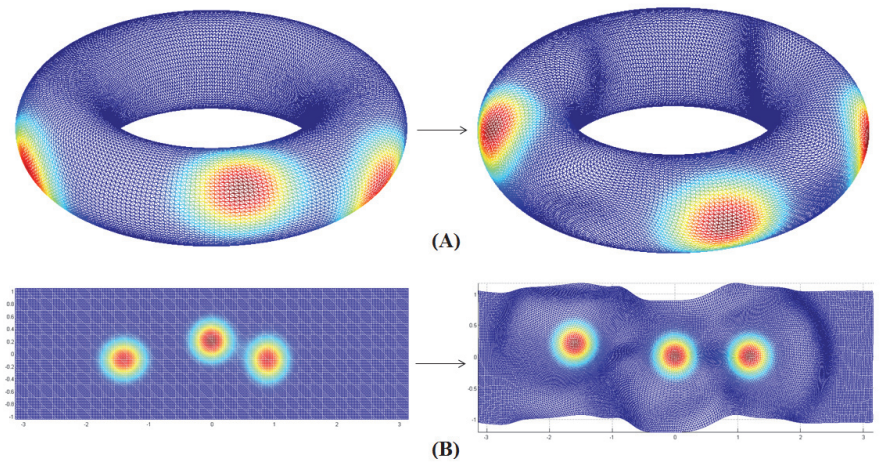

Figure 5. (A) *shows the registration result that matches the intensity function. The intensity function defined on* S_1 *is mapped to* S_2 *using the obtained registration.* (B) *shows the registration result on the universal covering spaces. Note that the boundary cuts are not fixed. They move freely on the universal covering space and while satisfying the periodic conditions.*

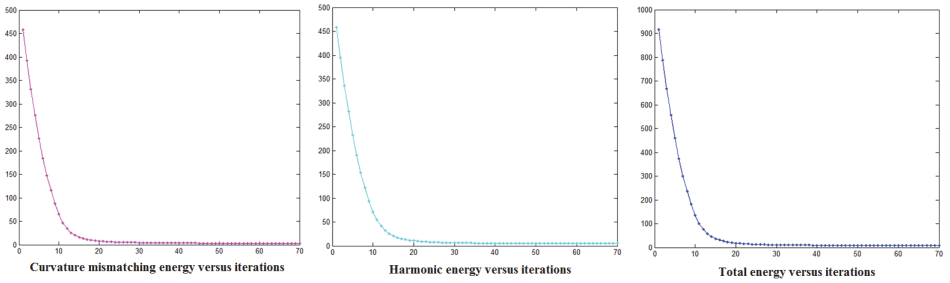

Figure 6. *The intensity mismatching energy, harmonic energy, and total energy versus iterations for the geometric registration problem in Figure* 5.

matches the intensity functions. The intensity function defined on S_1 is mapped to S_2 using the obtained registration. (B) shows the registration result on the universal covering spaces. The intensity functions are perfectly matched under the obtained registration (compared with Figure 4(D)). Note that the boundary cuts are not fixed. They move freely on the universal covering space of S_2 and while satisfying the periodic conditions. Figure 6 shows the intensity mismatching energy, harmonic energy, and total energy versus iterations. All of them decrease monotonically as the iteration increases. It demonstrates that our algorithm computes the optimized (Euclidean) harmonic map between the two genus-1 surfaces that matches the intensity functions as much as possible.

Example 2. We test our proposed algorithm to obtain geometric matching registration between two synthetic genus-1 surfaces through matching their curvatures. Figures 7(A) and (B) show two synthetic genus-1 surfaces, with three bumps added to each surface located at different positions. The colormaps on each surfaces are given by their mean curvatures.

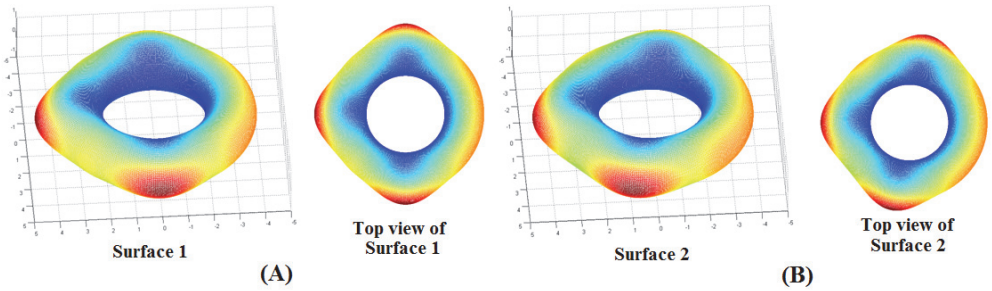

Figure 7. *Two synthetic genus-*1 *surfaces are shown in* (A) *and* (B)*, respectively. Two bumps are added to each surface at different locations. The colormap is given by the mean curvature.*

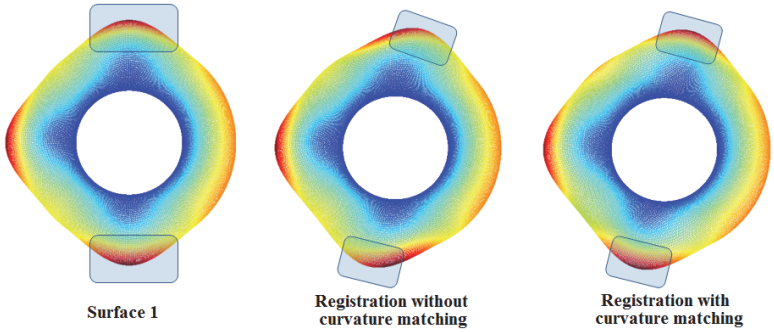

Figure 8. *The results of registration without curvature matching and with curvature matching are shown in the figure. The color intensity on surface* 1 *(given by the mean curvature) is mapped to surface* 2 *using the obtained registrations. The registration without curvature matching cannot match the feature bumps on the two surfaces, whereas the registration with curvature matching can match the bumps consistently.*

Using our proposed method, we compute both the registration without curvature matching and the registration with curvature matching. The registration result is shown in Figure 8. The color intensity on S_1 (given by the mean curvature) is mapped to S_2 using the obtained registrations. The registration without curvature matching cannot match the feature bumps on the two surfaces, whereas the registration with curvature matching can match the bumps consistently. It illustrates that our proposed method can obtain a better registration that matches the geometry between the two surfaces. The curvature mismatching energy, harmonic energy, and total energy versus iterations are shown in Figure 9. Again, all energies decrease monotonically as the iteration increases and converge in about 30 iterations.

Example 3. We next test our algorithm on synthetic genus-2 surfaces. Figures 10(A) and (B) show two genus-2 surfaces, denoted by S_1 and S_2, respectively, with different intensity functions defined on each of them. The two surfaces are parameterized onto their universal covering spaces, and registration between the two surfaces is computed on the 2D parameter domains. The intensity functions on each surface are plotted on their universal covering spaces, which are shown in (C) and (D). In Figure 11(A), we show the obtained registration between the two surfaces that matches the intensity functions. The intensity function defined on S_1 is mapped to S_2 using the obtained registration. (B) shows the registration result

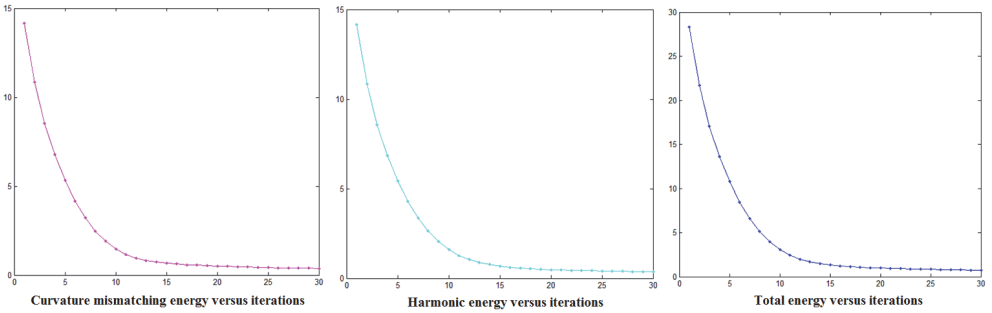

Figure 9. *The curvature mismatching energy, harmonic energy, and total energy versus iterations for the geometric registration problem in Figure 8.*

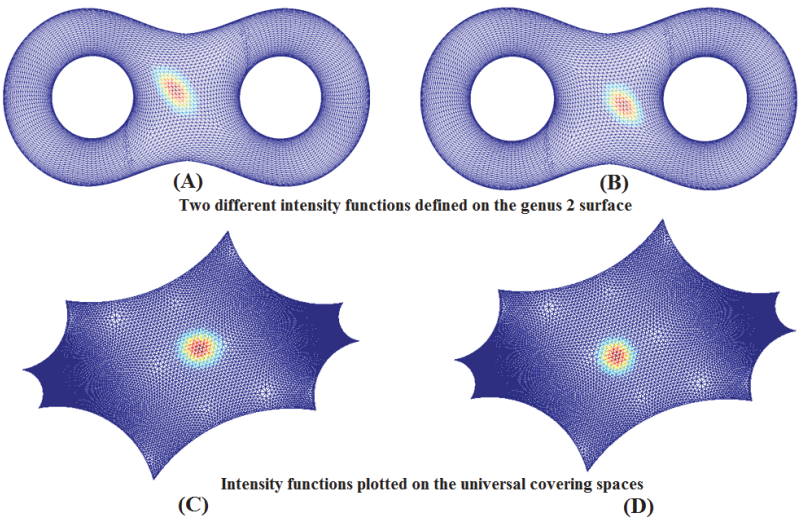

Figure 10. (A) *and* (B) *show two genus-2 tori with different intensity functions defined on each of them.* (C) *and* (D) *show the intensity functions plotted on the universal covering spaces of* (A) *and* (B)*, respectively.*

on the universal covering spaces. The intensity functions are perfectly matched under the obtained registration (compared with (D)). Again, the boundary cuts are not fixed. They move freely on the universal covering space of S_2 and while satisfying the periodic conditions. Figure 12 shows the intensity mismatching energy, harmonic energy, and total energy versus iterations. All of them decrease monotonically as the iteration increases. It illustrates that our algorithm computes the optimized (hyperbolic) harmonic map between the genus-2 surfaces that matches the intensity functions as much as possible.

Example 4. We also test our method on two synthetic genus-2 surfaces. Figures 13(A) and (B) show two synthetic genus-2 surfaces, with two bumps added to each surface located at different positions. The colormaps on each surface are given by their mean curvatures. Using our proposed method, we compute both the registration without curvature matching and the registration with curvature matching. The registration results are shown in Figure 14. The color intensity on S_1 (given by the mean curvature) is mapped to S_2 using the obtained

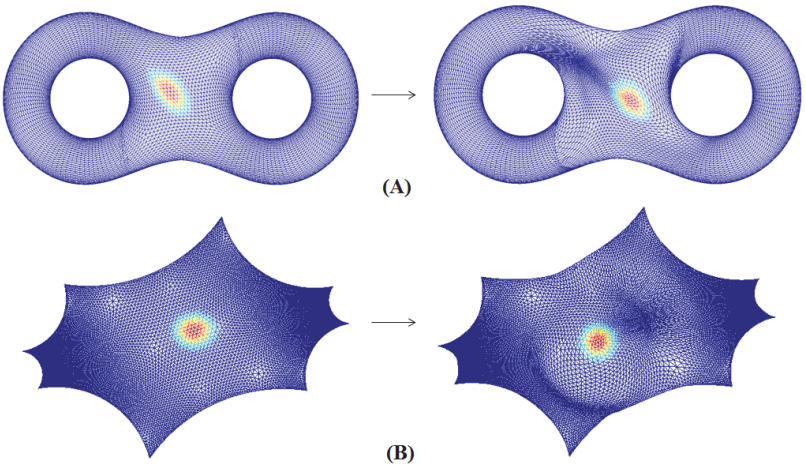

Figure 11. (A) *shows the registration result that matches the intensity function. The intensity function defined on* S_1 *is mapped to* S_2 *using the obtained registration.* (B) *shows the registration result on the universal covering spaces. Note that the boundary cuts are not fixed. They move freely on the universal covering space and while satisfying the periodic conditions.*

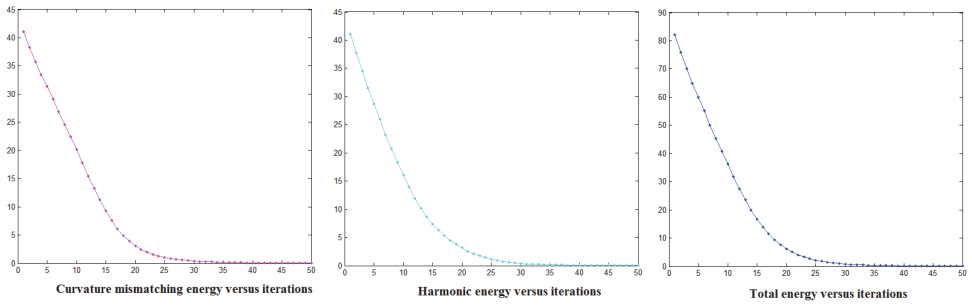

Figure 12. *The intensity mismatching energy, harmonic energy, and total energy versus iterations for the geometric registration problem in Figure* 11.

registrations. The registration without curvature matching cannot match the feature bumps on the two surfaces (see the regions in the highlighted boxes). It is, however, observed that the registration with curvature matching can match the bumps consistently. It again demonstrates the effectiveness of our proposed method for obtaining a geometric matching registration between genus-2 surfaces. Figure 15 shows the curvature mismatching energy, harmonic energy, and total energy versus iterations. Again, all energies decrease monotonically as the iteration increases and converge in about 20 iterations.

6.2. Real medical data. In medical imaging, studying shape changes of anatomical structures is important for the purpose of disease analysis. To perform shape analysis effectively, an accurate surface registration between anatomical structures is necessary. In this subsection, we will show two applications of our proposed algorithm in medical imaging for registering two real medical data, namely, the vertebrae bone and the vestibular system.

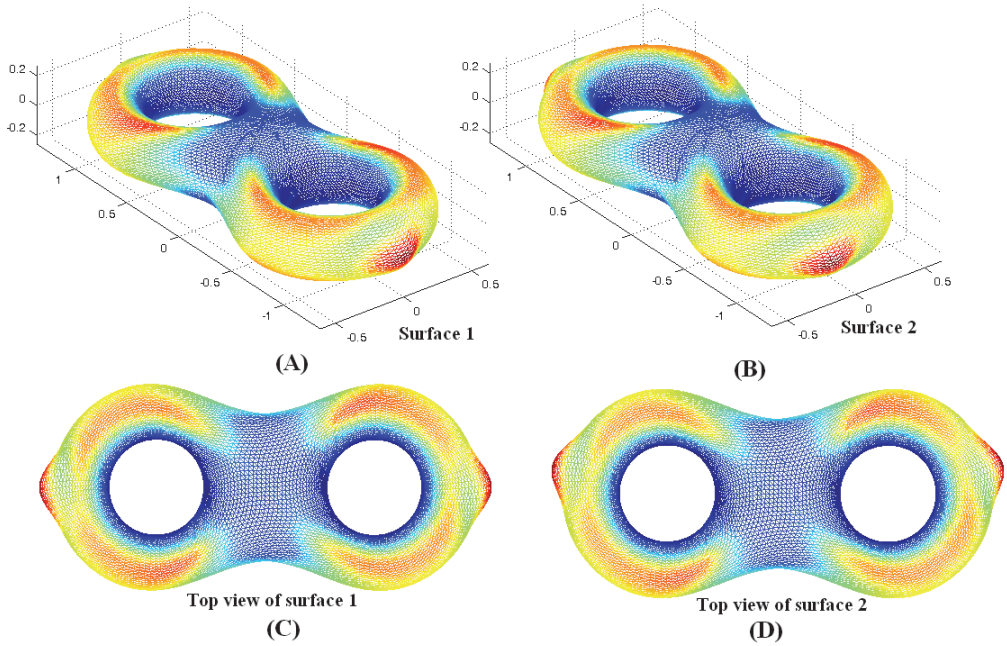

Figure 13. *Two synthetic genus-2 surfaces are shown in* (A) *and* (B)*, respectively. Two bumps are added to each surface at different locations. The colormap is given by the mean curvature.* (C) *and* (D) *show the top view of the two surfaces.*

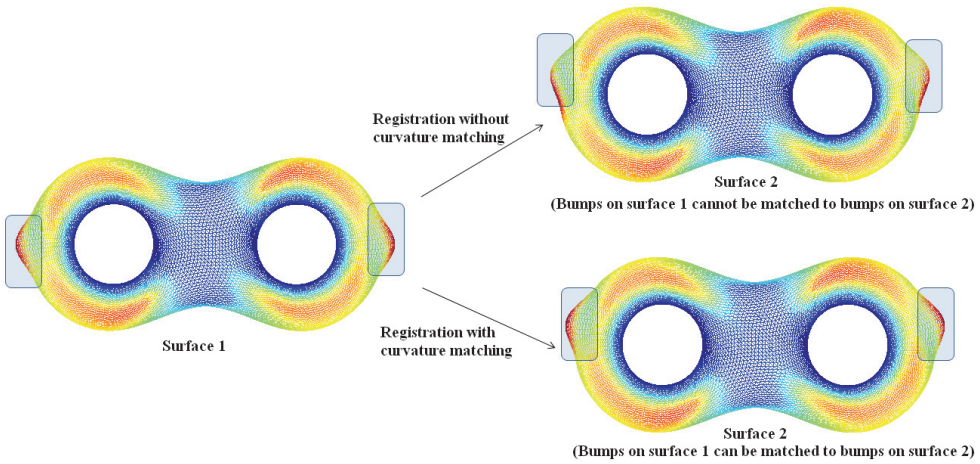

Figure 14. *The results of registration without curvature matching and with curvature matching are shown in the figure. The color intensity on surface* 1 *(given by the mean curvature) is mapped to surface* 2 *using the obtained registrations. The registration without curvature matching cannot match the feature bumps on the two surfaces, whereas the registration with curvature matching can match the bumps consistently.*

Example 5 *(vertebrae bone).* The study of morphological changes of the vertebrae is important in detecting vertebral fractures and degenerative shape changes. An accurate and meaningful registration between the vertebrae bone surfaces is therefore important. Using

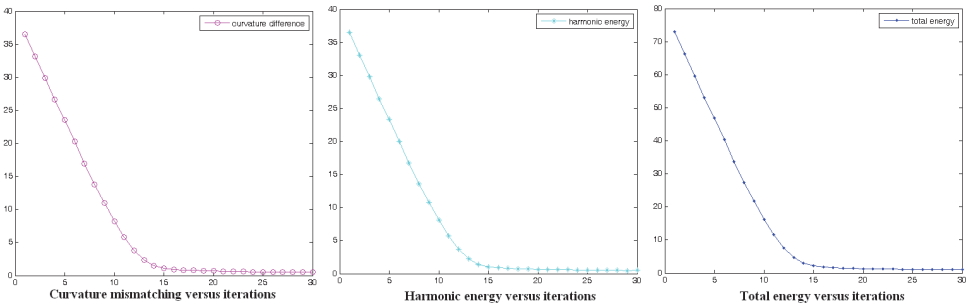

Figure 15. *The curvature mismatching energy, harmonic energy, and total energy versus iterations for the geometric registration problem in Figure 14.*

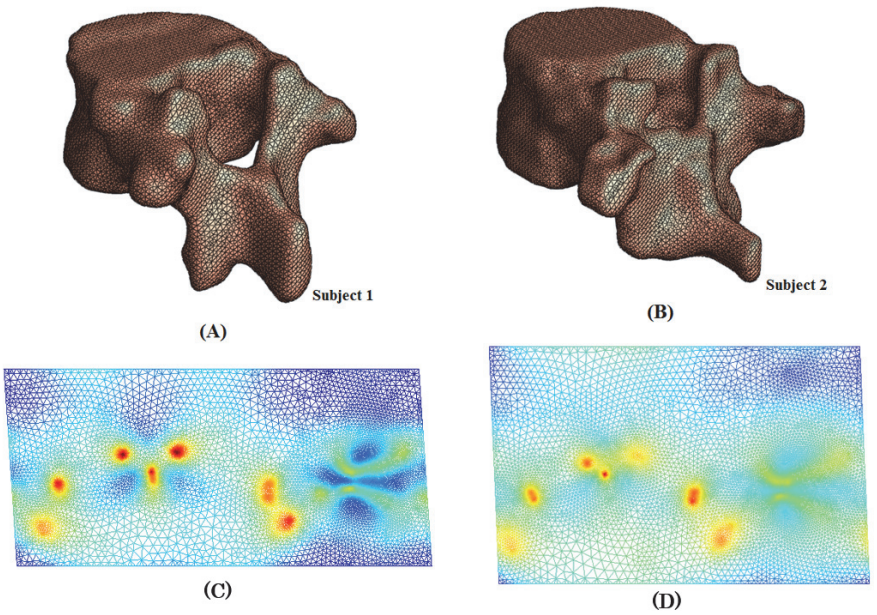

Figure 16. (A) *and* (B)*: The vertebrae bones of genus one of two different subjects.* (C) *and* (D) *show the mean curvature functions plotted on the universal covering spaces of* (A) *and* (B).

our proposed algorithm, a geometric matching surface registration between different vertebrae bones can be obtained. Figures 16(A) and (B) show the vertebrae bones of two different subjects. They are both of genus one. Their mean curvature functions on each surface are plotted on their universal covering spaces, which are shown in (C) and (D). Our goal is to find a geometric matching registration between the two surfaces.

The registration result of the vertebrae bones using our proposed algorithm is shown in Figure 17. (A) shows the vertebrae bone surface of Subject 1, colored by its mean curvature. The color intensity (given by the mean curvature) on the vertebrae bone of Subject 1 is mapped to the vertebrae bone of Subject 2 in (B), using the obtained registration. Note that the high curvature regions are consistently matched. For example, the "hammers" on the vertebrae bone of Subject 1 (labeled as regions I–V) are matched consistently with the

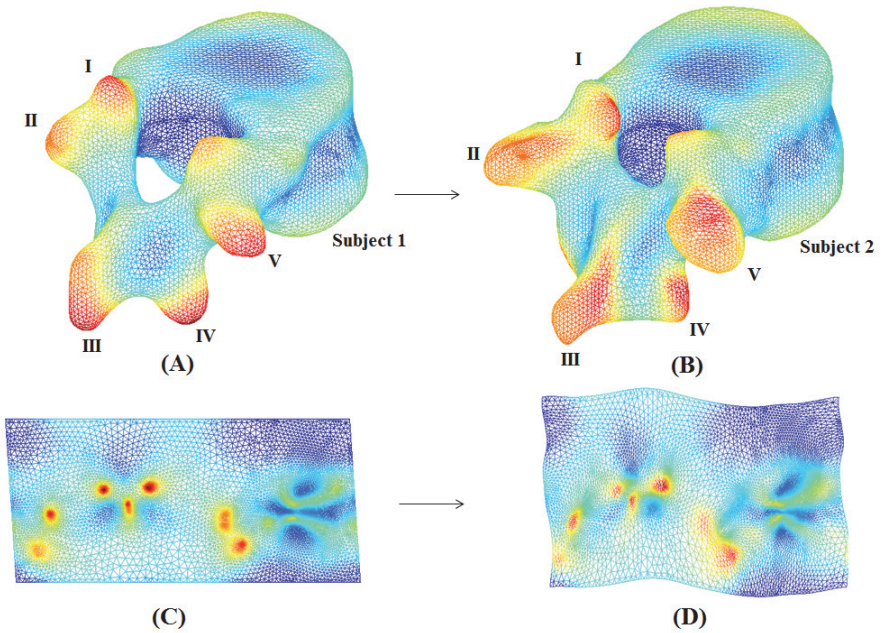

Figure 17. *The registration result of the vertebrae bones using our proposed algorithm.* (A) *shows the vertebrae bone surface of Subject* 1*, colored by its mean curvature. The color intensity (given by the mean curvature) on the vertebrae bone of Subject* 1 *is mapped to the vertebrae bone of Subject* 2 *in* (B)*, using the obtained registration. Note that the high curvature regions are consistently matched.* (C) *and* (D) *show the registration result on the universal covering spaces.*

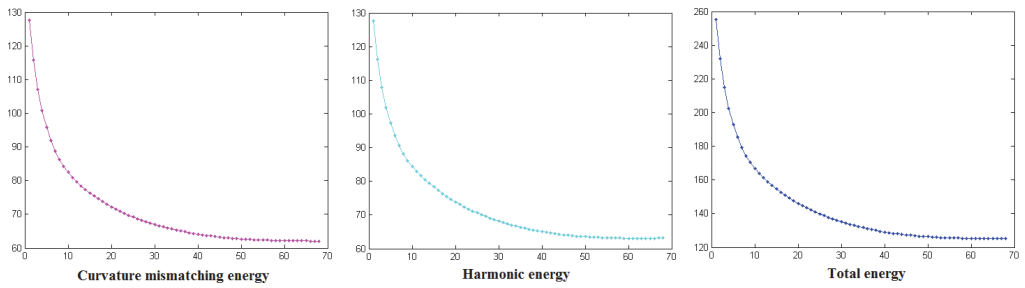

Figure 18. *The curvature mismatching energy, harmonic energy, and total energy versus iterations for the geometric registration problem in Figure* 17*.*

"hammers" on the vertebrae bone of Subject 2. (C) and (D) show the registration result on the universal covering spaces. Note that the boundary cuts are not fixed. They move freely on the universal covering space and while satisfying the periodic conditions.

Figure 18 shows the curvature mismatching energy, harmonic energy, and total energy versus iterations of our algorithm. All energies monotonically decrease as the iteration increases. In particular, the curvature mismatching energy decreases monotonically, which means the optimal map obtained matches curvatures as much as possible.

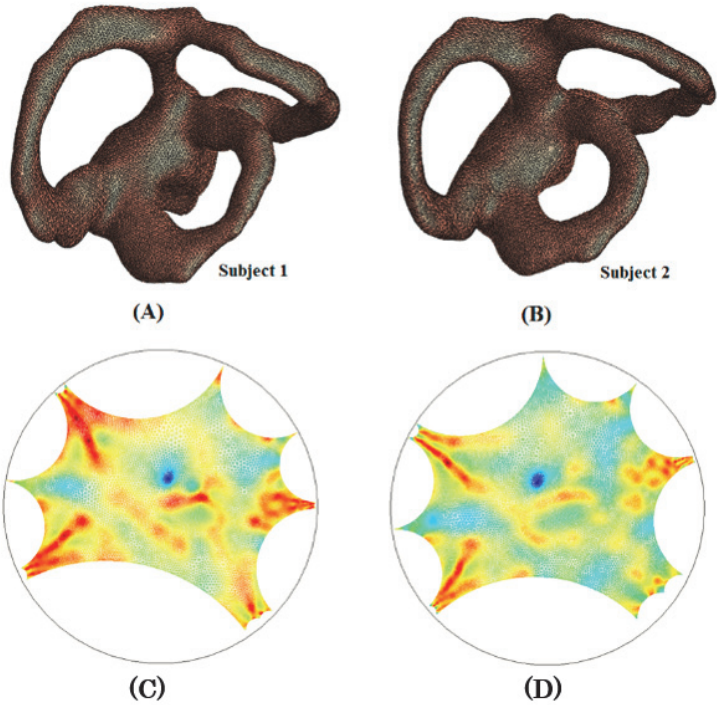

Figure 19. (A) *and* (B)*: The VSs of genus three of two different subjects.* (C) *and* (D) *show the mean curvature functions plotted on the universal covering spaces of* (A) *and* (B).

Example 6 *(vestibular system).* The vestibular system (VS) is an inner structure of the ear, which is responsible for perception of head movements and sending postural signals to the brain. The shape analysis of the VS plays an important role in understanding a disease called adolescent idiopathic scoliosis (AIS), which is a three dimensional spinal deformity affecting about 4% schoolchildren worldwide [38, 39]. It therefore calls for the need to register the VSs. The VS is of genus three. The high-genus topology of the surface poses great challenges for obtaining the surface registration.

Using our proposed algorithm, we obtain a geometric matching surface registration between the VSs. Figures 19(A) and (B) show the VSs of two different subjects. They are both of genus three. Their mean curvature functions on each surface are plotted on their universal covering spaces, which are shown in (C) and (D). Our goal is to find a geometric matching registration between the two surfaces.

The registration result of the VSs using our proposed algorithm is shown in Figure 20. (A) shows the VS of Subject 1, colored by its mean curvature. The color intensity (given by the mean curvature) on the VS of Subject 1 is mapped to the VS of Subject 2 in (B), using the obtained registration. Note that the corresponding regions are consistently matched. For example, the three canals of each surface are matched consistently. (C) and (D) show the registration result on the universal covering spaces. Note that the boundary cuts are not fixed. They move freely on the universal covering space and while satisfying the periodic

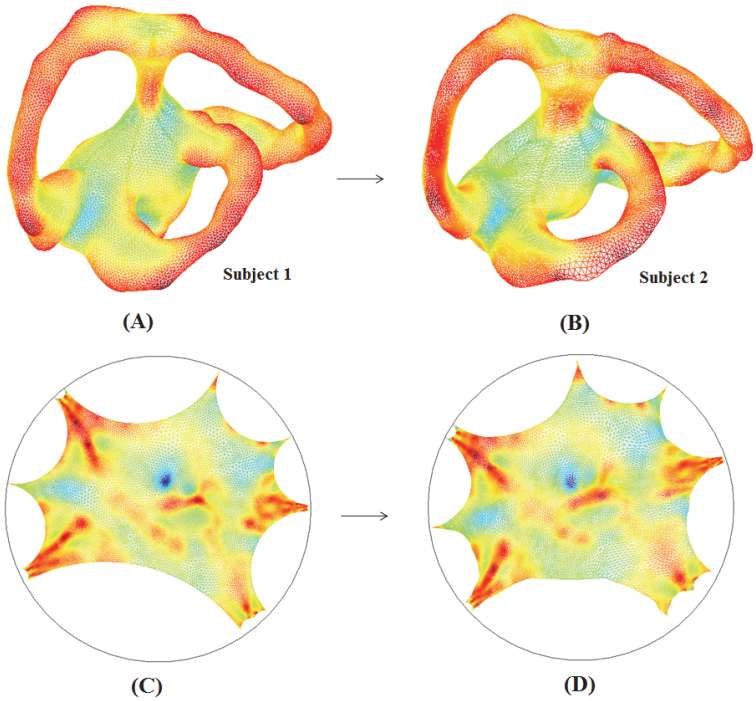

Figure 20. *The registration result of the VS using our proposed algorithm.* (A) *shows the VS surface of Subject* 1*, colored by its mean curvature. The color intensity (given by the mean curvature) on the VS of Subject* 1 *is mapped to the VS of Subject* 2 *in* (B)*, using the obtained registration. Note that the corresponding regions are consistently matched.* (C) *and* (D) *show the registration result on the universal covering spaces.*

conditions. In other words, it is not necessary to introduce consistent cuts on the two surfaces in our algorithm.

7. Conclusion and future works. In this work, we propose a method to obtain geometric registrations between high-genus ($g \geq 1$) surfaces, without introducing consistent cuts. The key idea is to conformally parameterize the surface into its universal covering space in $\mathbb{R}^2$. Registration can then be done on the universal covering by minimizing a shape mismatching energy measuring the geometric dissimilarity between the surfaces. Our proposed algorithm effectively computes a smooth registration between high-genus surfaces that matches geometric information as much as possible. To test the performance of the proposed method, numerical experiments have been done on synthetic high-genus surface data. Results show that our proposed algorithm is effective in registering high-genus surfaces with complete geometric matching. The proposed method has also been applied to registration of anatomical structures for medical imaging, which demonstrates the usefulness of the proposed algorithm. In the future, we will apply the proposed algorithm to register more anatomical structures, such as the VS and the vertebrae bone, for the purpose of disease analysis.

Acknowledgment. The medical data were provided by CUHK Medical School.

REFERENCES

[1] S. Haker, S. Angenent, A. Tannenbaum, R. Kikinis, G. Sapiro, and M. Halle, *Conformal surface parameterization for texture mapping*, IEEE Trans. Visual. Comput. Graph., 6 (2000), pp. 181–189.

[2] O. Lyttelton, M. Boucher, S. Robbins, and A. Evans, *An unbiased iterative group registration template for cortical surface analysis*, NeuroImage, 34 (2007), pp. 1535–1544.

[3] F. Gardiner and N. Lakic, *Quasiconformal Teichmuller Theory*, American Mathematical Society, Providence, RI, 2000.

[4] B. Fischl, M. Sereno, R. Tootell, and A. Dale, *High-resolution intersubject averaging and a coordinate system for the cortical surface*, Hum. Brain Mapp., 8 (1999), pp. 272–284.

[5] X. Gu, Y. Wang, T. F. Chan, P. M. Thompson, and S.-T. Yau, *Genus zero surface conformal mapping and its application to brain surface mapping*, IEEE Trans. Med. Imag., 23 (2004), pp. 949–958.

[6] Y. Wang, L. M. Lui, X. Gu, K. M. Hayashi, T. F. Chan, A. W. Toga, P. M. Thompson, and S.-T. Yau, *Brain surface conformal parameterization using Riemann surface structure*, IEEE Trans. Med. Imag., 26 (2007), pp. 853–865.

[7] X. Gu and S. Yau, *Computing conformal structures of surfaces*, Commun. Inf. Syst., 2 (2002), pp. 121–146.

[8] S. Joshi and M. Miller, *Landmark matching via large deformation diffeomorphisms*, IEEE Trans. Image Process., 9 (2000), pp. 1357–1370.

[9] A. M. Bronstein, M. M. Bronstein, A. M. Bruckstein, and R. Kimmel, *Analysis of two-dimensional non-rigid shapes*, Int. J. Comput. Vis., 78 (2008), pp. 67–88.

[10] Y. Lipman and I. Daubechies, *Conformal Wasserstein distances: Comparing surfaces in polynomial time*, Adv. Math., 227 (2011), pp. 1047–1077.

[11] Y. Lipman, J. Puente, and I. Daubechies, *Conformal Wasserstein distance:* II. *Computational aspects and extensions*, Math. Comp., 82 (2013), pp. 331–381.

[12] J. Glaunès, M. Vaillant, and M. I. Miller, *Landmark matching via large deformation diffeomorphisms on the sphere*, J. Math. Imaging Vision, 20 (2004), pp. 179–200.

[13] J. Glaunes, L. Younes, and A. Trouve, *Diffeomorphic matching of distributions: A new approach for unlabelled point-sets and sub-manifolds matching*, in Proceedings of the IEEE Conference on Computer Vision and Pattern Recognition (CVPR'04), Vol. 2, 2004, pp. 712–718.

[14] J. Glaunes, A. Qiu, M. Miller, and L. Younes, *Large deformation diffeomorphic metric curve mapping*, Int. J. Comput. Vis., 80 (2008), pp. 317–336.

[15] J. Glaunes, A. Qiu, M. Miller, and L. Younes, *Surface matching via currents*, in Proceedings of Information Processing in Medical Imaging (IPMI'05), Vol. 3565, 2005, pp. 381–392.

[16] M. K. Hurdal and K. Stephenson, *Discrete conformal methods for cortical brain flattening*, NeuroImage, 45 (2009), pp. 86–98.

[17] N. A. Lord, J. Ho, B. C. Vemuri, and S. Eisenschenk, *Simultaneous registration and parcellation of bilateral hippocampal surface pairs for local asymmetry quantification*, IEEE Trans. Med. Imag., 26 (2007), pp. 471–478.

[18] B. T. Yeo, M. R. Sabuncu, T. Vercauteren, N. Ayache, B. Fischl, and P. Golland, *Spherical demons: Fast diffeomorphic landmark-free surface registration*, IEEE Trans. Med. Imag., 29 (2010), pp. 650–668.

[19] F. L. Bookstein, *Principal warps: Thin-plate splines and the decomposition of deformations*, IEEE Trans. Pattern Anal. Mach. Intell., 11 (1989), pp. 567–585.

[20] T. Vercauteren, X. Pennec, A. Perchant, and N. Ayache, *Diffeomorphic demons: Efficient non-parametric image registration*, NeuroImage, 45 (2009), pp. S61–S72.

[21] Y. Wang, L. Lui, T. Chan, and P. Thompson, *Optimization of brain conformal mapping with landmarks*, in Proceedings in Medical Image Computing and Computer-Assisted Intervention (MICCAI), 2005, pp. 675–683.

[22] L. Lui, S. Thiruvenkadam, Y. Wang, T. Chan, and P. Thompson, *Optimized conformal parameterization of cortical surfaces using shape based matching of landmark curves*, in Proceedings in Medical Image Computing and Computer-Assisted Intervention (MICCAI), 2005, pp. 494–502.

[23] L. M. Lui, S. Thiruvenkadam, Y. Wang, P. M. Thompson, and T. F. Chan, *Optimized conformal*

surface registration with shape-based landmark matching, SIAM J. Imaging Sci., 3 (2010), pp. 52–78.
[24] L. Lui, Y. Wang, T. Chan, and P. Thompson, *Landmark constrained genus zero surface conformal mapping and its application to brain mapping research*, Appl. Numer. Math., 57 (2007), pp. 847–858.
[25] L. M. Lui, Y. Wang, T. F. Chan, and P. M. Thompson, *Brain anatomical feature detection by solving partial differential equations on general manifolds*, Discrete Contin. Dyn. Syst. Ser. B, 7 (2007), pp. 605–618.
[26] L. M. Lui, T. W. Wong, X. F. Gu, T. F. Chan, and S. T. Yau, *Compression of surface diffeomorphism using Beltrami coefficient*, in Proceedings of the IEEE Conference on Computer Vision and Pattern Recognition (CVPR'10), 2010, pp. 2839–2846.
[27] L. M. Lui, T. W. Wong, W. Zeng, X. F. Gu, P. M. Thompson, T. F. Chan, and S. T. Yau, *Optimization of surface registrations using Beltrami holomorphic flow*, J. Sci. Comput., 50 (2012), pp. 557–585.
[28] W. Zeng, L. M. Lui, F. Luo, T. F. Chan, S. T. Yau, and X. F. Gu, *Computing quasiconformal maps using an auxiliary metric and discrete curvature flow*, Numer. Math., 121 (2012), pp. 671–703.
[29] L. M. Lui, T. W. Wong, X. F. Gu, P. M. Thompson, T. F. Chan, and S. T. Yau, *Hippocampal shape registration using Beltrami holomorphic flow*, in Proceedings in Medical Image Computing and Computer Assisted Intervention (MICCAI), Part II, Lecture Notes in Comput. Sci. 6362, Springer, Berlin, 2010, pp. 323–330.
[30] L. M. Lui, K. C. Lam, T. W. Wong, and X. F. Gu, *Texture map and video compression using Beltrami representation*, SIAM J. Imaging Sci., 6 (2013), pp. 1880–1902.
[31] O. Lehto and K. Virtanen, *Quasiconformal Mappings in the Plane*, Springer-Verlag, New York, 1973.
[32] R. Schoen and S.-T. Yau, *Lectures on Differential Geometry*, International Press, Boston, 1994.
[33] D. Tosun, M. Rettmann, and J. Prince, *Mapping techniques for aligning sulci across multiple brains*, Med. Image Anal., 8 (2004), pp. 295–309.
[34] J. Erickson and K. Whittlesey, *Greedy optimal homotopy and homology generators*, in Proceedings of the Sixteenth Annual ACM-SIAM Symposium on Discrete Algorithms, 2005, pp. 1038–1046.
[35] M. Jin, J. Kim, F. Luo, and X. Gu, *Discrete surface Ricci flow*, IEEE Trans. Visual. Comput. Graph., 14 (2008), pp. 1030–1043.
[36] Y. L. Yang, J. Kim, F. Luo, S. Hu, and X. F. Gu, *Optimal surface parameterization using inverse curvature map*, IEEE Trans. Visual. Comput. Graph., 14 (2008), pp. 1054–1066.
[37] T. Lin, C. L. Guyader, I. Dinov, P. Thompson, A. Toga, and L. Vese, *Gene expression data to mouse atlas registration using a nonlinear elasticity smoother and landmark points constraints*, J. Sci. Comput., 50 (2012), pp. 586–609.
[38] W. Zeng, L. M. Lui, L. Shi, D. Wang, W. C. W. Chu, J. C. K. Cheng, X. F. Gu, and S. T. Yau, *Shape analysis of vestibular systems in adolescent idiopathic scoliosis using geodesic spectra*, in Proceedings in Medical Image Computing and Computer Assisted Intervention (MICCAI), Part III, Lecture Notes in Comput. Sci. 6363, Springer, Berlin, 2010, pp. 538–546.
[39] S. Xin, Y. He, P. Fu, L. Shi, D. Wang, W. C. W. Chu, J. C. K. Cheng, X. F. Gu, and L. M. Lui, *Euclidean geodesic loops on high-genus surfaces applied to the morphometry of vestibular systems*, in Proceedings in Medical Image Computing and Computer Assisted Intervention (MICCAI), 2011, pp. 384–392.